8-2019

Pipeline for Variable Star Detection and Eclipsing Binary Characterization

Moises Castillo
The University of Texas Rio Grande Valley

PIPELINE FOR VARIABLE STAR DETECTION AND ECLIPSING BINARY CHARACTERIZATION

A Thesis

by

MOISES CASTILLO

Submitted to the Graduate College of
The University of Texas Rio Grande Valley
In partial fulfillment of the requirements for the degree of

MASTER OF SCIENCE

August 2019

Major Subject: Physics

PIPELINE FOR VARIABLE STAR DETECTION AND ECLIPSING BINARY CHARACTERIZATION

A Thesis
by
MOISES CASTILLO

COMMITTEE MEMBERS

Dr. Mario C. Diaz
Chair of Committee

Dr. Nicolas Pereyra
Committee Member

Dr. Andreas Hanke
Committee Member

August 2019

ABSTRACT

Castillo, Moises, Pipeline for variable star detection and eclipsing binary characterization. Master of Science (MS), August, 2019, 63 pp., 4 tables, 36 figures, 44 references.

Stars have been observed and recorded since ancient times. Practices of documenting brightness led to observations of variability. Optical CCD observations of eclipsing binary stars were made with instruments at UTRGV Dr. Cristina Valeria Torres Memorial Astronomical Observatory. There are two main goals for this project. The first goal is to create a pipeline written in python (lightcurator) that creates a framework for detecting variable stars. The pipeline starts by creating a list of ccd frames written in FITS format of an eclipsing binary star observation. These object frames are expected to be already reduced, but lightcurator provides tools to achieve this. The object frames are aligned and stacked to create a deepsky frame. Astrometry is performed to find the proper positions in right ascension and declination of all sources in the deepsky frame. This creates a master catalogue of stars to be monitored through the entire observation. Source extraction is performed on each object frame to generate a catalogue of stars that includes the measure of instrumental flux and the time recorded. After converting instrumental flux to instrumental magnitude, light curves are produced for every object for all frames. Currently, lightcurator is limited to detecting cataloged variable stars from the General Catalogue of Variable Stars (GCVS) and the Variable Star Index (VSX). Identification of the intended eclipsing binary system is confirmed in all cases with this method. The second goal for this project is to extract the physical parameters of the eclipsing binary systems observed from the time series data computed from the pipeline.

DEDICATION

This is dedicated to my mom, Kiryat, and dad, Alfredo.
Gracias por sus consejos, enseñanzas y todo el amor.

To my brother, Joe, who supports me no matter what I do.

To my sister, Kitty, who continues to march foward
to the beat of her own drum.

To my love, Samantha, for always motivating me to
move foward with what I believe in and for caring for me
no matter how busy you are. I love you.

To who ever may read this,
may it provide inspiration for you to do great things.

-Moises

ACKNOWLEDGMENTS

I would like to acknowledge Mario Claudio Diaz for his continued support not only as an academic and research advisor, but a mentor in life. Also for entrusting me with the keys of the observatory that allowed this project to exist. Richard Camuccio for teaching me what he knows of observatories, astronomy, and instrumentation. Also for sharing expeiences that helped us grow as academics, researchers, and humans. Martin Beroiz for your seemingly infinite wealth of knowledge in everything. Your guidance and perspective helped me in classes and research. And your work has inspired me to work harder. The late Cristina Valeria Torres for her compassion in public outreach, teaching, and learning. Her words of advice as a mentor and friend have helped me form decisions regarding academia and life.

The CTMO Team and GAIA for trusting my foward thinking and believing, together, we can make our observatory autonomous. This allowed me to push this project foward. Carlos Colazo, Raul Melia, and Carla Giardini, for teaching me the fundamentals of becoming an observational astronomer through practice and many hours of working in the dark. The Center for Gravitational Wave Astronomy for financial support. Soma Mukherjee, Ivan Davila, and Blanca Garcia for assisting me through the administrative requirements to meet the criteria for acceptance. Andreas Hanke, Nicolas Pereyra, and Natalia Guevara for agreeing to help my thesis process rapidly and unconditionally. Americo Hinojosa Lee for providing me assitance in fufilling GAIA duties while I worked on my thesis. Pawan Kumar Thapalia for showing me the LaTeX template activley maintained by Guillermo Garza of UTRGV-SMSS.

This research has made use of the VizieR catalogue access tool, CDS, Strasbourg, France. The original description of the VizieR service was published in A&AS 143, 23. This research made use of ccdproc, an Astropy package for image reduction (Craig et al. 2017).

TABLE OF CONTENTS

Page

LIST OF TABLES

Page

LIST OF FIGURES

Page

CHAPTER I

INTRODUCTION

1.1 Variable stars

Stars are called variable when there is a detectable change in brightness or color on time scales of the order of the mean life time of humans [24, 36]. The first claimed documented variable star is Algol visible with the unaided eye. There exists ancient Egyptian calendars of lucky and unlucky days that possibly contain the periodicity of Algol[29, 30]. The Cairo Calendar dated to 1244–1163 BC has been shown by Porceddu et al. [20] to represent Algol as Horus, a sky god and symbol of kingship, as seen in the Figure 1.1 by matching the actions of Horus and the events witnessed by an observer of Algol.

There is some curious relation between ancient Greek stories of the Gorgon Medusa, Perseus, the corresponding constellations, and the variable stars Algol and Omicron Ceti or more commonly named Mira (the wonderful). Wilk [42] suggests that the variability and location in the sky is embedded within the stories themselves.

The first recognized documented variable star, Omicron Ceti, was recorded in 1596 and again in 1609 by David Fabricius while observing Jupiter. Fabricius had first recorded Omicron Ceti as a nova, a singular event observed as a bright flash and quick dimming over the next few days, comparing its significance with a supernova recorded by Tycho Brahe in 1572. In 1638, Omicron Ceti was rediscovered by Johannes Phocylides Holwarda who found the periodic nature of this star to be approximately 11 months [16].

Figure 1.1: Inside the rectangle is the hieratic writing for the word Horus [20].

1.2 Classifying variability

Over time there have been several attempts to classify variable stars. Classification systems reflect the current understanding of the mechanisms behind variability. The earliest variable star observers like Goodricke and Pigott, who was employed to verify the variability of stars [26], would try to make sense of the observations and periods recorded by comparing and grouping different stars to those like Algol and o Ceti.

One of the first attempts that went into detail was made by E. C. Pickering [17, 36] in 1881 where he classified variable stars into the following categories[25]:

Type I Temporary stars. Examples, Tycho Brahe's star of 1572, new star in Corona, 1866.

Type II Stars undergoing great variations in light in periods of several months or years. Examples, o Ceti and χ Cygni.

Type III Stars undergoing slight changes according to laws yet unknown

Type IV Stars whose light is continually varying, but the changes are repeated with great regularity in a period not exceeding a few days.

Type V Stars which every few days undergo for a few hours a remarkable diminution in light, this phenomenon recurring with great regularity.

As time passes with more observations of variable stars, the collective understanding of the mechanisms of variability are improved. With an improved understanding of physical processes including stellar evolution, pulsation, rotation, and eclipsing, then the taxonomy of classes is refined.

Since 1946, on behalf of the International Astronomical Union (IAU), Moscow variable star researchers have compiled detailed catalogs and certified variable stars in the General Catalogue of Variable Stars (GCVS). GCVS 5.1 is the most current version of the catalog containing $52,011$ variable objects discovered and named as variable stars by 2015 [34].

1.2.1 General Catalogue of Variable Stars 5.1 Variability Types

Variability types are in groups according to the major astrophysical reasons for variability. The variable types have letter designations that typically corresponds to the original star that is observed with the same type of variability. For example, in the eruptive group there is a type called GCAS that signifies eruptive irregular variables of the Gamma Cas type. The definitions of the variable types are given by GVCS and maintained on their website: `http://www.sai.msu.su/gcvs/gcvs/`

The following are groups with the variable types in those groups. The reader can visit the

GCVS Variability Types webpage[1] to see specific variable types.

eruptive FU, GCAS, I, IA, IB, IN, INA, INB, INT, IT, IN (YY), IS, ISA, ISB, RCB, RS, SDOR, UV, UVN, WR,

pulsating ACYG, BCEP, BCEPS, CEP, CEP (B), CW, CWA, CWB, DCEP, DCEPS, DSCT, DSCTC, GDOR, L, LB, LC, M, PVTEL, RPHS, RR, RR (B), RRAB, RRC, RV, RVA, RVB, SR, SRA, SRB, SRC, SRD, SXPHE, ZZ, ZZA, ZZB,

rotating ACV, ACVO, BY, ELL, FKCOM, PSR, SXARI,

cataclysmic (explosive and novalike) variables N, NA, NB, NC, NL, NR, SN, SNI, SNII, UG, UGSS, UGSU, UGZ, ZAND,

eclipsing binary systems E, EA, EB, EW, GS, PN, RS, WD, WR, AR, D, DM, DS, DW, K, KE, KW, SD,

intense variable X-ray sources X, XB, XF, XI, XJ, XND, XNG, XP, XPR, XPRM, XM,

other symbols BLLAC, CST, GAL, L:, QSO, S, *, +, :

the new variability types ZZO, AM, R, BE, LBV, BLBOO, EP, SRS, LPB

This document will not cover all the different variable stars types. The study specifically will focus on EW type eclipsing binary systems.

[1]GCVS Variability Types: `http://www.sai.msu.su/gcvs/gcvs/vartype.htm`

CHAPTER II

ECLIPSING BINARY SYSTEMS

2.1 Defining eclipsing binary system

As the name implies, an eclipsing binary system is such that at least two objects orbit close to the same plane as viewed from an observer on Earth so that one object eclipses the other.

2.2 Eclipsing binary system types

Eclipsing binary systems are classified into three sub group types. The following are the eclipsing binary system types and definitions set by the GCVS:

2.2.1 Classification based on the shape of the light curve

E Eclipsing binary systems. These are binary systems with orbital planes so close to the observer's line of sight (the inclination i of the orbital plane to the plane orthogonal to the line of sight is close to 90 deg) that the components periodically eclipse each other. Consequently, the observer finds changes of the apparent combined brightness of the system with the period coincident with that of the components' orbital motion.

EA Algol (Beta Persei)-type eclipsing systems. Binaries with spherical or slightly ellipsoidal components. It is possible to specify, for their light curves, the moments of the beginning and end of the eclipses. Between eclipses the light remains almost constant or varies insignificantly because of reflection effects, slight ellipsoidality of components, or physical variations. Secondary minima may be absent. An extremely wide range of periods is observed, from 0.2 to >= 10000 days. Light amplitudes are also quite different and may reach several magnitudes.

EB Beta Lyrae-type eclipsing systems. These are eclipsing systems having ellipsoidal components and light curves for which it is impossible to specify the exact times of onset and end of eclipses because of a continuous change of a system's apparent combined brightness between eclipses; secondary minimum is observed in all cases, its depth usually being considerably smaller than that of the primary minimum; periods are mainly longer than 1 day. The components generally belong to early spectral types (B-A). Light amplitudes are usually <2 mag in V.

EP Stars showing eclipses by their planets. Prototype: V0376 Peg.

EW W Ursae Majoris-type eclipsing variables. These are eclipsers with periods shorter than 1 days, consisting of ellipsoidal components almost in contact and having light curves for which it is impossible to specify the exact times of onset and end of eclipses. The depths of the primary and secondary minima are almost equal or differ insignificantly. Light amplitudes are usually <0.8 mag in V. The components generally belong to spectral types F-G and later.

2.2.2 Classification according to the components' physical characteristics

GS Systems with one or both giant and supergiant components; one of the components may be a main sequence star.

PN Systems having, among their components, nuclei of planetary nebulae (UU Sge).

RS RS Canum Venaticorum-type systems. A significant property of these systems is the presence in their spectra of strong Ca II H and K emission lines of variable intensity, indicating increased chromospheric activity of the solar type. These systems are also characterized by the presence of radio and X-ray emission. Some have light curves that exhibit quasi sine waves outside eclipses, with amplitudes and positions changing slowly with time. The presence of this wave (often called a distortion wave) is explained by differential rotation of the star, its surface being covered with groups of spots; the period of the rotation of a spot

group is usually close to the period of orbital motion (period of eclipses) but still differs from it, which is the reason for the slow change (migration) of the phases of the distortion wave minimum and maximum in the mean light curve. The variability of the wave's amplitude (which may be up to 0.2 mag in V) is explained by the existence of a long-period stellar activity cycle similar to the 11-year solar activity cycle, during which the number and total area of spots on the star's surface vary.

WD Systems with white-dwarf components.

WR Systems having Wolf-Rayet stars among their components (V 444 Cyg).

2.2.3 Classification based on the degree of filling of inner Roche lobes

AR Detached systems of the AR Lacertae type. Both components are subgiants not filling their inner equipotential surfaces.

D Detached systems, with components not filling their inner Roche lobes.

DM Detached main-sequence systems. Both components are main-sequence stars and do not fill their inner Roche lobes.

DS Detached systems with a subgiant. The subgiant also does not fill its inner critical surface.

DW Systems similar to W UMa systems in physical properties (KW, see below), but not in contact.

K Contact systems, both components filling their inner critical surfaces.

KE Contact systems of early (O-A) spectral type, both components being close in size to their inner critical surfaces.

KW Contact systems of the W UMa type, with ellipsoidal components of F0-K spectral type. Primary components are main-sequence stars and secondaries lie below and to the left of the main sequence in the (MV,B-V) diagram.

SD Semidetached systems in which the surface of the less massive component is close to its inner Roche lobe.

The combination of the above three classification systems for eclipsers results in the assignment of multiple classifications for object types. These are separated by a solidus ("/") in the data field. Examples are: E/DM, EA/DS/RS, EB/WR, EW/KW, etc.

2.3 Eclipsing Binary Characterization

Binary stars can reveal physical properties by examining the light curves.

2.4 Light curve

A light curve is a plot of brightness vs time. Variations in brightness must be allowed due to changes in the optical path rather than from the source. The specific methods on considering the tolerance will be discussed in Chapter IV.

The method for calculating the physical parameters from light curve data that is commonly used in eclipsing binary research is called WD Code.

2.5 WD code

Current models use a process first developed by Wilson and Devinney in 1971 [43] for studying close eclipsing binary systems now called WD code.

In this study a modified WD code is used called PHOEBE (Physics of Eclipsing Binaries) code. The current release PHOEBE 2.1 [18] was built upon the previous releases 2.0 [33] and the original legacy code [32].

CHAPTER III

INSTRUMENTATION

The author is leading the Group for the Advancement in Automation and Instrumentation (GAIA). GAIA is the group responsible for maintaining, servicing, and upgrading hardware and software related to the observatory.

3.1 Dome

Dr. Cristina Valeria Torres Memorial Astronomical Observatory (CTMO) inaugurated May 5, 2018. Formerly Nompuewenu Observatory. The word Nompuewenu meaning “beyond the sky” is borrowed from the Mapuche language used by the Mapuche people indigenous to Argentina.

The observatory was first constructed on the Brownsville campus of UTRGV. With a growing downtown and campus light pollution became a serious issue for the observatory. Alumn Antonio Galan scouted the region for a suitable location to relocate. Former State Park Superintendent Pablo Deyturbe found Galan scouting the area near Resaca de la Palma State Park (RDLP). Director of the Center for Gravitational Wave Astronomy (CGWA) Mario Diaz and Deyturbe worked together to establish a Memorandum of Understanding between UTRGV and Texas Parks and Wildlife Department (TPWD) to allow the relocation of the observatory to be Resaca de la Palma State Park.

The dome is a custom build with all parts manufactured uniquely for this research and educational facility.

3.1.1 Specifications

Observatory style Dome shape

Figure 3.1: Dr. Cristina Valeria Torres Memorial Astronomical Observatory at Resaca de la Palma State Park photo by Americo Hinojosa Lee

Window Two parts, upper slides along domed roof; bottom opens draw bridge style

Wall height 88 inches

Average Diameter 245 inches[1]

Approximate Height 25 feet

3.1.2 Robotizing of dome for remote operation

The author is leading efforts to robotize the observatory and instrumentation for remote and autonomous operation. The motors that control the shutter door and rotation are controlled manually. For optimal control of the observatory, robotizing these controls is required. These are the planned upgrades for the observatory.

[1] Average diameter is used since all domes increase in eccentricity or become egg shaped over time

- Add hydraulic lift system to control shutter draw bridge door
- Implement wireless communication for shutter window and door control
- Add gear encoding to dome rotation motor using a rotary sensor
- Add cardinal position encoding using permanent magnets and hall effect sensors
- Use scripts to create nightly observation queues based on requests and LIGO[2] alerts for Optical Followups of Gravitational Wave Events
- Develop drivers for communicating with sensors and observatory software

3.1.3 Hardware

The author has created prototypes of sensors to use for gear encoding with optical and hall effect sensors.

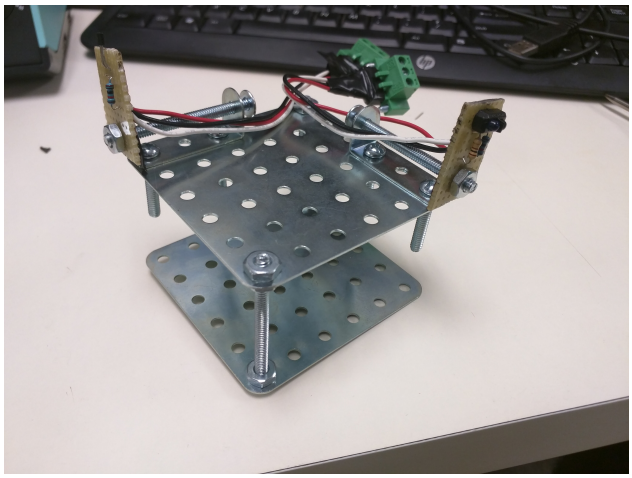

Figure 3.2: Two sensors on mounting stage to be installed on observatory wall. Left: hall effect sensor. Right: optical sensor.

- Dome Rotation
  - Arduino Uno
  - Yaskawa J1000 Drive

[2]Laser Interferometer Gravitational Wave Observatory

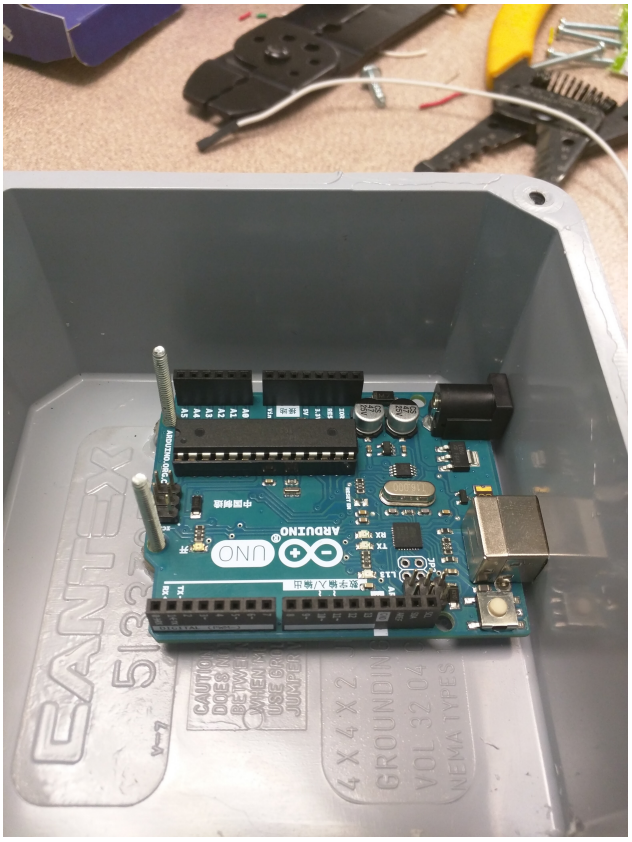

Figure 3.3: Arduino Uno inside enclosure

  - Custom Relay Circuit

- Shutter Control Window
  - 12 VDC Gel Marine Battery
  - Custom Controller

- Shutter Drawbridge
  - Rope
  - Pulley

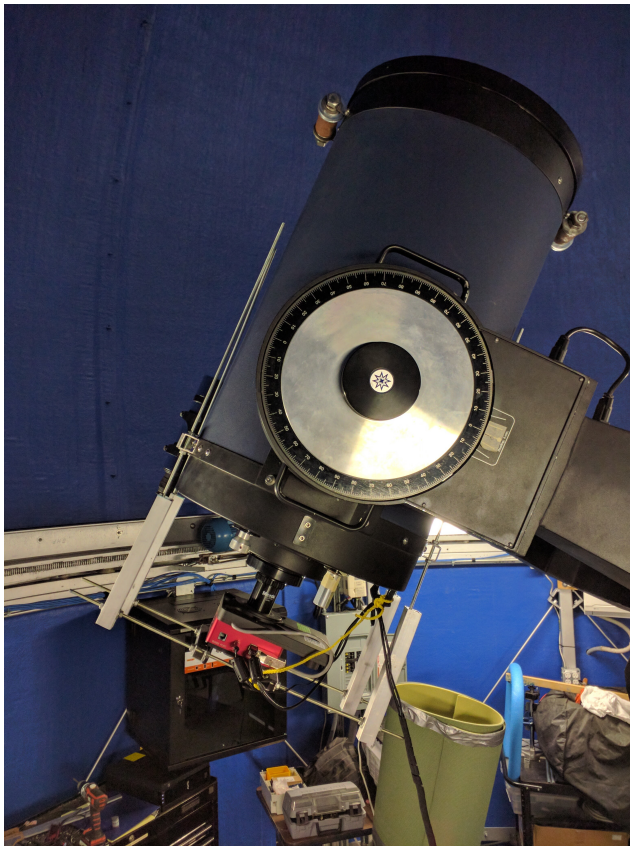

Figure 3.4: 16-in Meade LX200-GPS

3.2 Telescope System

3.2.1 16-inch Meade LX200-GPS

OTA Specifications The following specifications are given by the manufacturer Meade Instruments Corporation [11] for the optical tube assembly (OTA).

Optical design Schmidt-Cassegrain

Clear aperture 406.4 mm

Focal length 4064 mm

Focal ratio f/10

Resolving power 0.28″

Coatings Meade EMC Super Multi-Coatings

Mounting Heavy-duty double-tine forks

Gears 11-inch diameter worm gears, both axes

Periodic error correction Both axes

Alignment Alt-Azimuth or equatorial with optional pier

Pointing Precision 2′ in GO TO mode

Slew Speeds 1x sidereal to 8 deg/s in 9 increments

Power 18V power supply

Accesories These are devices used during regular observations or setup

- 8x 50 mm viewfinder
- 4-speed zero image-shift microfocuser
- 16-channel GPS receiver
- True-level electronic sensor

Net telescope weight 110 lbs

Telescope Pier Telescope pier was constructed by a custom pedestal and the optional equatorial wedge made by Meade.

Pedastal height 44.25 inches

Wedge height 32 inches

Wedge inclination 26 deg

Weight 225 lbs

Installation Installation required multiple steps. First, using a chain winch we set the pedestal onto bolts that were installed in the base of the concrete pad designed for the load of the telescope. Second, using the winch we installed the pier on top of the pedestal keeping alignment of the wedge due north for polar alignment of the telescope. Third, using the winch we lifted the telescope to the wedge and bolted the instrument.

A special bolting technique was used to allow for precise polar alignment.

Limitations Exposures longer than 30 seconds were not possible due to noticeable drift. Attempts were made to correct for this issue by doing a drift polar alignment.

The microfocuser was not able to hold the weight of the cameras used for research. The author designed and constructed a rig pictured in figure 3.5 that fit on the back of the OTA that supported the extra weight and allowed for regular function of the microfocuser.

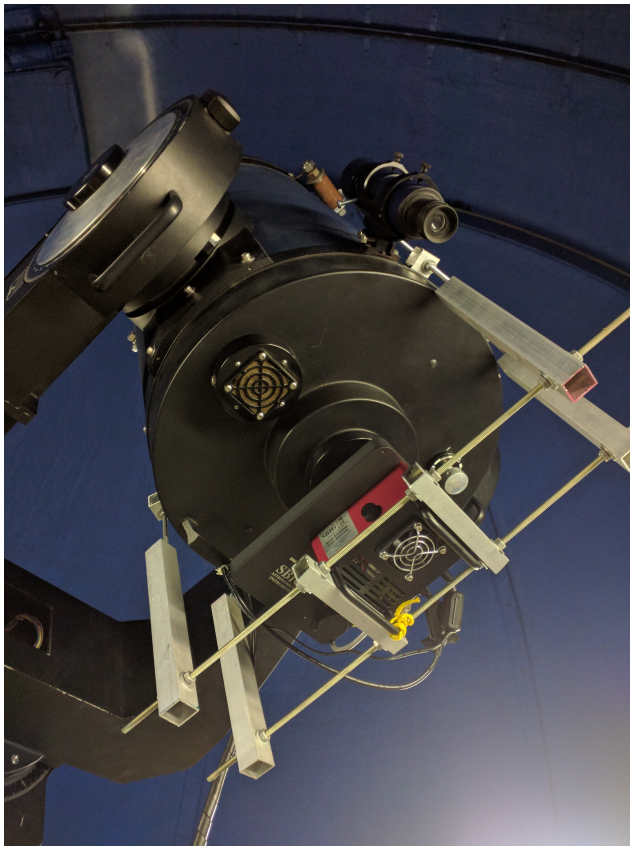

Figure 3.5: Rig that was designed and constructed by the author shown supporting SBIG STF8300 behind 16-in Meade LX200-GPS

3.2.2 CDK17 on L-500 direct drive mount

Specifications The following specifications are given by the manufacturer PlaneWave Instruments [27] for the optical tube assembly (OTA).

Optical design Corrected Dall-Kirkham

Aperature 432 mm

Focal length 2939 mm

Focal ratio F/6.8

OTA Weight 106 lbs

OTA length 1067 mm

Feature Three cooling fans ejecting air from the back of the telescope and four fans blowing across the boundary layer of the mirror surface. This helps the telescope to reach thermal equilibrium quickly. The fans are controlled by a computer if the optional Electronic Focus Accessory (EFA Kit) is purchased.

Mounting L-500 direct drive mount

Mount weight 257 lbs

Load Capacity 200 lbs

Slew Rate 20 degrees per second (standard); 50 degrees per second (maximum), both axes

Motor Control Industrial grade brushless motor control system and built in electronics

Pointing Accuracy $<$ 10 arcsecond RMS with PointXP Model

Pointing Precision 2 arcsecond

Tracking Accuracy $<$ 0.3 arcsecond error over 5 minute period

System Natural Frequency 10 Hz or greater

Telescope Pier The manufacturer Planewave Instruments provided a tool for calculating the required pier height for their wedge and L-500 Direct Drive Mount. We used the same pedestal that was used with the Meade pier.

Figure 3.6: Pedestal, pier, and wedge before installation of mount

Pedastal height 44.25 inches

Wedge inclination for latitudes 22–28 degrees

Wedge weight 145 lbs

Pier height 12 inches

Installation The installation of the CDK17 with L-500 mount required the removal of the 16-inch Meade LX200 GPS Telescope system and wedge from the pedestal. After removal of the Meade system, we installed the 12-inch pier on the pedestal. Over the pier we installed

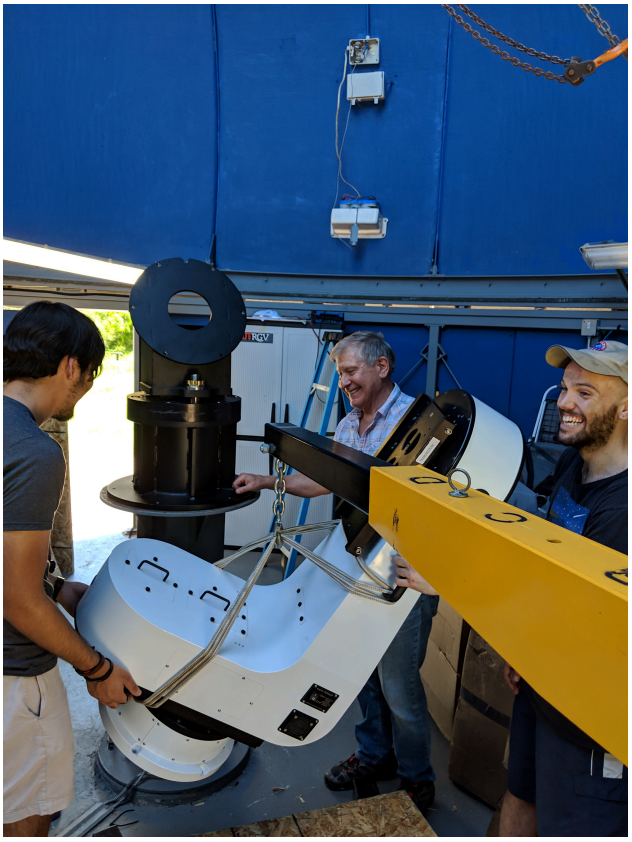

Figure 3.7: Installation of CDK500

the wedge and did a rough alignment to due north for polar alignment. Precision was not critical at this point since the Planewave wedge for L500 mount features fine latitude and azimuth adjustments. We used a combination of a winch and motor hoist crane to support the weight of the L-500 mount to bolt the mount to the wedge. Finally, we adjusted the saddle of the telescope and fit onto the mount.

Prior to use, balancing was done with the camera and focuser installed. The manufacturer had to remotely recalibrate the motors due to the weight of instrumentation.

Pointing model is required for proper pointing. This was created following a process in PWI3, software developed by Planewave. First, 30 evenly spaced point above 30 degrees in altitude were selected. The software commands the telescope to one of 30 points, takes a picture, finds the positions of all objects in the frame through a process called plate solving to establish precise pointing position, and updates the table of the pointing to the plate solved position.

Limitations We have found no issues with drifting with exposures longer than 2 minutes and tracking holding steady for over 4 hours.

3.3 Camera

3.3.1 Pixel Scale

Pixel scale is a conversion between the angular distance of sky that is visible per pixel. Chromey [10] describes pixel scale as,

$$\text{pixel scale} = \frac{206,265}{f} d \tag{3.1}$$

where f is the focal is the focal length and d is the separation between the centers of pixels. For our calculations, we will assume d is equal to the pixel width.

3.3.2 Field of View

Field of view (FOV) refers to the angular distance of sky that is visible through the telescope given the physical parameters of the CCD. FOV can be calculated by the following equation as described by Chromey [10],

$$\text{FOV} = (\text{pixel scale})(\text{length}) \times (\text{pixel scale})(\text{width}) \tag{3.2}$$

3.3.3 SBIG STF-8300

The following specifications are given by the manufacturer Diffraction Limited [35].

Specifications

CCD Kodak KAF-8300

Pixel Size $5.4 \times 5.4\,\text{m}$

Pixel Array 3326×2504 pixels

CCD Size $17.96 \times 13.52\,\text{mm}$

Gain $0.37\,e-/\text{ADU}$

Read noise $9.3\,e$

Digitization Rates 10 Megapixels / Second

Full Frame Download Less than 1 second

Weight 1.8 pounds

Linearity tests of the SBIG STF-8300 have been performed and documented by Camuccio [6] to measure gain and read noise. A plot of the mean pixel value vs the exposure time is show in figure 3.8.

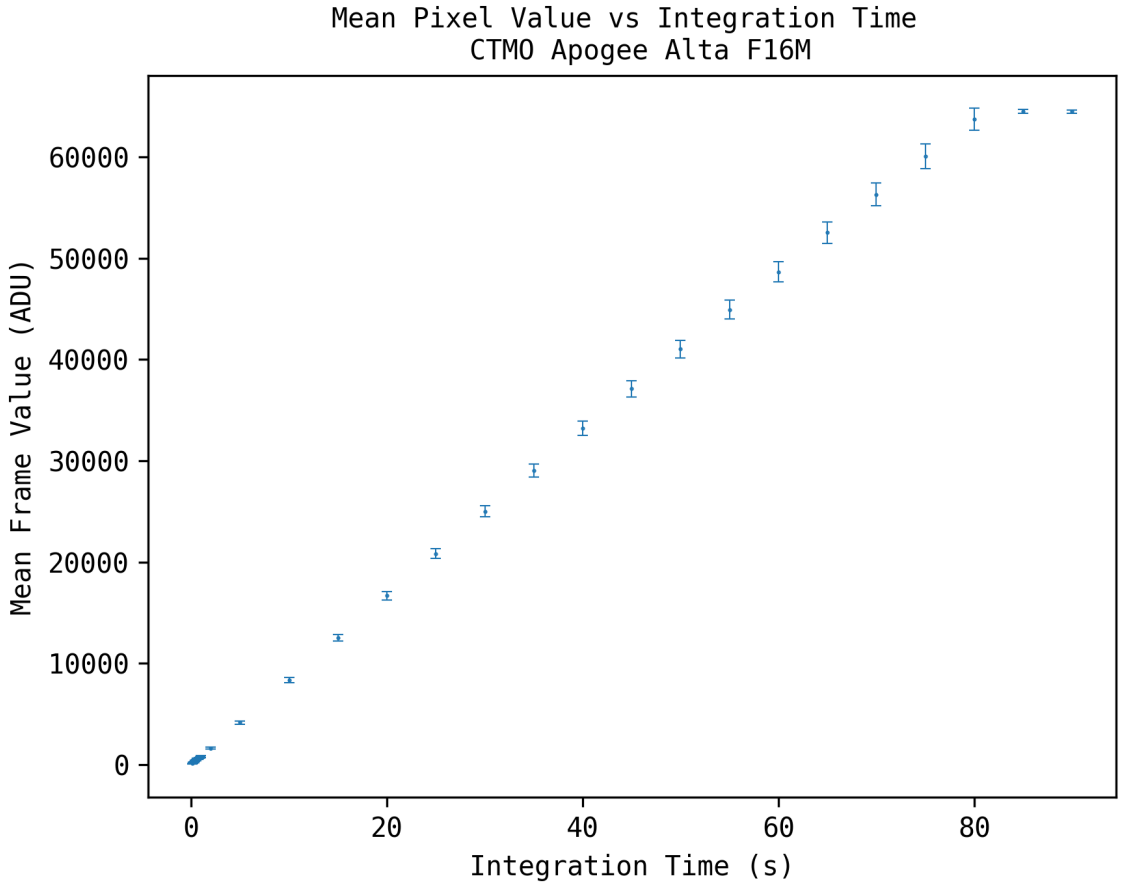

Figure 3.8: Linearity test of SBIG SFT-8300 performed by Richard Camuccio [6]

16-inch Meade Using equations 3.1 and 3.2 to find pixel scale and FOV, respectively, we find,

Pixel scale $0.274''$/pixel

FOV $15.19' \times 11.44'$

3.3.4 Apogee Alta F16M

Figure 3.9: Apogee Alta F16M being prepared for mounting onto CDK17

The following specifications are given by the manufacturer ANDOR [1].

Specifications

CCD Kodak KAF-16801

Pixel Size $9 \times 9\,\mu$m

Pixel Array 4096×4096 pixels

CCD Size 36.8×36.8 mm

Read noise $7.4\,e$

Weight 4.2 pounds

Linearity tests of the Apogee Alta have been performed and documented by Camuccio [6] to measure gain and read noise. A plot of the mean pixel value vs the exposure time is show in figure 3.10.

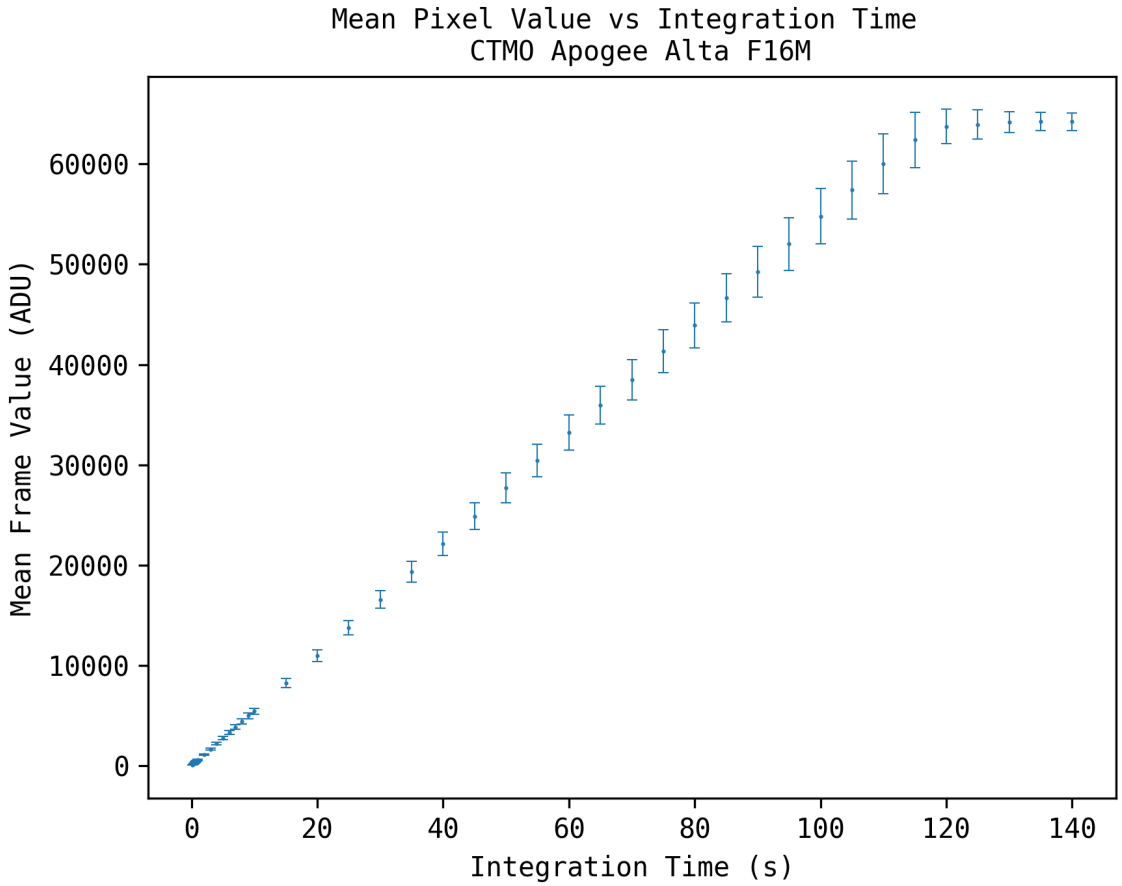

Figure 3.10: Linearity test of Apogee Alta performed by Richard Camuccio [6]

16-inch Meade Using equations 3.1 and 3.2 to find pixel scale and FOV, respectively, we find,

Pixel scale $0.457''$/pixel

FOV $31.18' \times 31.18'$

CDK17 Using equations 3.1 and 3.2 to find pixel scale and FOV, respectively, we find,

Pixel scale $0.63''$/pixel

FOV $43.12' \times 43.12'$

3.4 Software

CTMO has a Github page where software is being developed at `https://github.com/CTMObservatory` Software used was Maxim DL [13], Cartes du Ciel-The Sky [9], ASCOM Platform (POTH) [38], PWI3/PWI4[28], and INDI Library [19].

3.4.1 Dome

The author is leading the design and development of the custom software for the arduino. A custom ASCOM driver was written by Latifah Maasarani [22] to interface with an arduino. Arduino code is being written by Martin Beroiz.

3.4.2 Telescope

Maxim DL Used for 16-in Meade with ASCOM to attached WCS and pointing information to data

Cartes du Ciel Used for 16-in Meade with LX200 Driver and ASCOM Platform separately

PWI3 Used for focusing and controlling fans on CDK17

PWI4 Used for pointing CDK17

3.4.3 Camera

Maxim DL Used for controlling Camera coolers, Filter wheels, and plate solving.

3.4.4 Observatory Control System

This section explains the different observatory control systems implemented during use. Observatory controls unify the different hardware, drivers, and software. Use of systems like this allow for ease of use and proper storage of of data including World Coordinate System (WCS) attachment to the file headers of images.

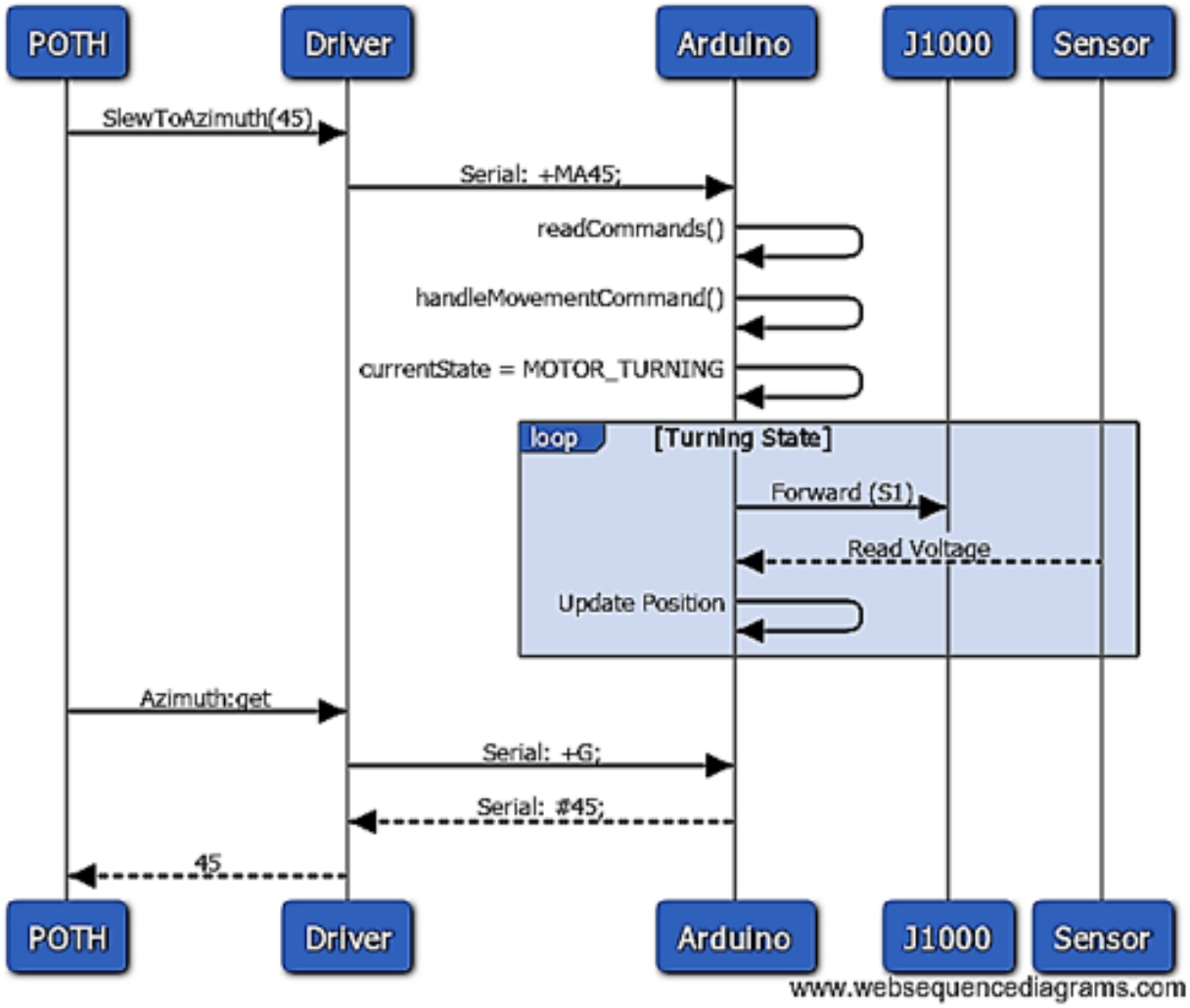

Figure 3.11: Sequence diagram for a movement command from POTH platform as implemented by Maasarani [22]

POTH POTH stands for Plain Old Telescope Handset. It uses a framework called ASCOM. ASCOM uses Windows COM protocols to communicate with the drivers required to operate equipment with the computer. POTH acts as a hub for all communications between drivers, devices, and programs to allow instruments to be used simultaneously on different programs.

INDI INDI stands for Instrument Neutral Distributed Interface. According to the INDI website[3], INDI Library is an open source architecture for control and automation of astronomical devices.

[3] `http://www.indilib.org`

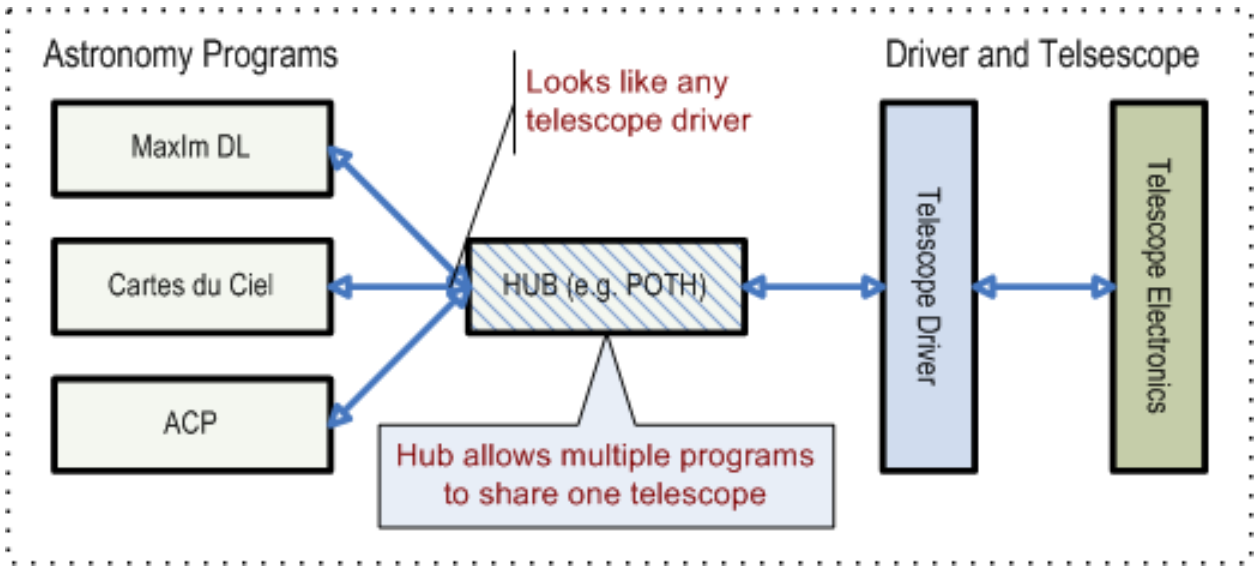

Figure 3.12: POTH block diagram of typical usage from ASCOM website [38]

3.4.5 POTH vs INDI

Both frameworks offer the same service, but were specific to operating system until more recently. INDI is working on a windows port, but it is in very early stages. There is a group called Cloudmakers[4] that made an INDI wrapper and server for Windows. The INDI wrapper bridges INDI commands with ASCOM protocols.

ASCOM now has an option for Unix based systems that works off of RESTful API and TCP/IP commands to communicate with drivers and clients called ASCOM Alpaca. According to the Alpaca developer's webpage[5], Alpaca is 100 percent independent of Windows. Nowhere in the Alpaca ecosystem is Windows (or COM) needed.

[4] http://www.cloudmakers.eu/windi/
[5] https://ascom-standards.org/Developer/Alpaca.htm

CHAPTER IV

METHODS

4.1 Data Acquisition

Eclipsing binary optical data acquisition requires an observer to do time series ccd photometry of one target with an observation cadence dependent on the period of the system. For example, the data gathered for this project was collected on multiple nights and observed on the order of hours with evenly timed frames.

4.1.1 Planning Observations

There are some options for selecting sources to observe. The following process is one learned in practice with amateur astronomer Carlos Colazo of Argentina. This study uses the Variable Star and Exoplanet Section of Czech Astronomical Society's observation project called BRNO Regional Network of Observers (BRNO) [40].

An ephemeris is made by using a table of predicted times of minima published on the BRNO webpage. For site specific predictions, the webpage needs to be visited in the original Czech language. A web form shown in figure 4.1 appears to include latitude and ELongitude (longitude in degrees east of the meridian) of the observation site.

It is important to mention the American Association of Variable Star Observers (AAVSO) offers a target tool on the web [1] to help make an observation plan.

Selection criteria Typically, EW type binary stars have the shortest period and were chosen for this reason. Observation time is set to start no later than one hour before the predicted time of minima. The error on the predicted time of minima can be great due to lack of observa-

[1] `https://filtergraph.com/aavso`

Figure 4.1: Web form for eclipsing binary predicted times of minima from the Variable Star and Exoplanet Section of Czech Astronomical Society's observation project called BRNO Regional Network of Observers (BRNO)

tional data.

BRNO classifies stars using a scale from 1 to 10. As a rule of thumb, the scale refers to the number of years since last reported observation. BRNO explicitly recommends observers observe objects with a rating of 5 or more.

Since observation are made over several hours it is best practice to pick objects on the eastern parts of the sky. This allows for maximum viewing time. The altitude of the target should be above 30 degrees for proper photometry study, but can be slightly lower.

Lastly, as with all observations, the limiting magnitude of the system will dictate what objects are observable. The change in magnitude of known eclipsing binaries stated in catalogs. The observer must make certain that the instrumentation allows for such observation. Millimagnitude precision is standard in exoplanet research, but is not required for any of the observations in this study.

4.1.2 Observation

When performing an eclipsing binary observation the observer should attempt to observe the same binary system through the entire night to capture the most complete period. Some systems need to be observed across several nights to obtain a full period. When conducting any measurement it is good practice to make plots on-the-fly to make sure the quality of data is consistent.

Since the observer typically will begin observation on the eastern sky with a low altitude, the air mass will be highest at the beginning of the observation. This can present a problem if the observer does not consider the increase of flux as the object approaches zenith or the highest point in the sky. When the object being observed reaches zenith, the air mass is the lowest and if not considered can cause over saturation of the CCD. Saturation is when the potential well for the pixel is completely filled and will no longer capture the electrons converted from the photon interaction with the CCD.

4.1.3 Post observation

After the observation is complete it is vital to collect calibration frames required for proper data reduction for photometry. Data reduction is the process for removing noise due to dark current, bias, and any obscuring defects in the optical path of the system. Required calibration frames are,

Flat Frames Flat frames are made by using an evenly illuminated light source. This can be created by using a white screen and a diffuse white light. This process will show any obscuring defects that are in the optical path like dust and vignetting. The required exposure time depends on the lighting system to reach a signal between 30 to 50 percent of saturation.

Dark Frames Dark frames are made by taking closed ‘exposures’ of the CCD. Exposure time for the dark frames need to match the flat frame exposure times and object exposure times.

Bias Frames Bias frames are only needed if the observer does not match the dark frame expo-

sure times to the flat frames. To take bias frames, the observer must take the shortest allowed exposure. Depending on software, by selecting the type of frame as bias, the exposure time will automatically be adjusted or displayed as zero.

4.2 Motivation for pipeline: lightcurator

Observing eclipsing binary systems especially of EW type require an observer to track the source on the order of hours. This means the data produced can include various stars as well as some potentially undiscovered variable stars. For this reason, the author created a python package called *lightcurator* [8] which is publicly available on Github `https://github.com/moemyself3/lightcurator` and on PyPI `https://pypi.org/project/lightcurator/` for easy installation using the package insaller for Python, *pip*. Lightcurator includes 2 packages: *lightcurve* and *calibration*. The functions included are described in the sections that follow. Future plans are documented as GitHub Issues and labeled as Enhancements [2].

4.3 Pipeline for variable star detection

1. Reduce data
2. Align frames
3. Create deepsky frame
4. Plate solve deepsky
5. Scrape deepsky header and add WCS to aligned frames
6. Extract sources from aligned frames
7. Extract sources from deepsky frame
8. Cross match sources from aligned frames to deepsky frame
9. Cross match master catalog with catalogs like VSX and GCVS

[2] The reader is encouraged to contribute to Enhancements and create pull requests.

10. Correct or normalize extracted flux data
11. Create or update database of previously observed sources
12. Plot individual light curves
13. Analyze individual light curves for variability estimation
14. Sort database given variability ranking

4.3.1 Data reduction

Reading, writing fits files, and creating data tables is done with a python package called *astropy* [2, 31]. Majority of the data reduction is done with astropy core package, coordinated packages, and affiliated packages. Coordinated packages are maintained by the Astropy Project and affiliated packages are not maintained by the Astropy Project, but is a part of the Astropy Project community.

Coordinated packages in use are *astroquery* [15], *ccdproc* [12], *photutils* [4]. An affiliated package in use is *astroscrappy* [23]. A package in the process of becoming an official affiliated package that is in use is *astroalign*. More details of astroalign are discussed in Section 4.3.2

Calibration Lightcurator has a module called calibration that provides the tools for convenient data reduction. The routine begins with the creating of the list of the fits files to be used with *ccdproc.ImageFileCollection*. The list is used for quick reference to all the fits files to be processed. The *validate_units* function checks for the fits keyword 'BUNIT'. If the units are missing then the function raises an exception and suggests to the user to use the *add_units* function. All the data sets including flats and darks collected at CTMO are missing units. This function inserts the 'BUNIT' keyword and sets the value to 'adu'.

After defining the paths to the location of the calibration files, i.e. flats and darks, running *create_masters* makes a master dark and master flat frame. This is done by doing a median combine of the dark frames. The dark frames are a measure of dark current which is the noise generated by the thermal energy generated by the silicon of the CCD. Since the CCD has a constant

voltage applied across the device, there is a bias in the signal generated that contains some read noise. By taking dark frames at the same exposure time as flat frames bias frames can be ignored since the noise will also be removed along with the dark frame.

The function *reduce* takes a user defined read noise, gain, and path to the directory containing the data to be reduced. The *reduce* function gain corrects the master dark and master flat then uses *ccdproc.ccd_process*. The *ccdproc.ccd_process* is an all-in-one function that gain corrects, dark subtracts, and flat corrects. It can also take into considerations uncertainties for error propagation, over scan regions, and any trimming that may be required in different set ups. The new reduced fits frames are then saved to file for later processing.

Through this process it is important to note that the file goes from storing 16-bit data to 64-bit data. This can easily cause a significant impact on a systems storage since the new frames are about 4 times larger than before.

Cosmic ray detection It is not uncommon to have cosmic rays hit the CCD causing peaks in signals that may be confused as sources during source extraction. The final step in data reduction is cosmic ray detection. For this, the function *ccdproc.cosmicray_lacosmic* identifies cosmic rays by identifying pixels based on a variation of Laplacian edge detection described by van Dokkum [39] and implemented by McCully in *astroscrappy* [23]. Lightcurator uses this algorithm with a function called *hotpixfix* prior to alignment of frames to allow a flexible approach by using raw frames instead of properly reduced frames.

4.3.2 Align frames

Frame alignment is done with a python package called *astroalign* written by Dr. Martin Beroiz [3] which is publicly available on Github[3]

Astroalign is the preferred method for image alignment since the raw data frames do not have World Coordinate System (WCS) information attached to the headers. WCS information encodes the transformations required to change x, y-pixel location to right ascension (RA) and declination (DEC).

[3]For the latest version of astroalign check: `https://github.com/toros-astro/astroalign`

Lightcurator uses a function called *try_register* to catch exceptions and reject by truncating the data frame if alignment cannot be completed. Exceptions from astroalign that are most commonly experienced are *MaxIterError* which is raised when the maximum number of iterations allowed by astroalign are met and a custom *Exception* raised when there are less than 3 sources detected.

Lightcurator assumes that there may be drift though the entire series of frames. For this reason, the frame in the middle of the time series is taken as the reference image.

4.3.3 Create deepsky frame

To create a deepsky frame a simple addition of all aligned frames are made. The CCD data is loaded into python as CCDData or numpy.ndarray types. Simple addition is used since the deepsky frame is only used for source detection and not for photometry. A more appropriate method for combining frames for photometry would be a median combine. This is not performed in this step since calculating the median would require more processing time and memory.

4.3.4 Plate solve deepsky

Plate solving is the process in which the exact position of the field is found by matching indexed data with the relative positions of the sources on the field in question.

Astrometery.net [21] is a service that exists online and as a standalone program that can solve the astrometry of a field.

Lightcurator acts as a wrapper that calls on the processes *solve-field* from astrometry.net. This starts the blind astrometric solving. If the fits header contained pointing information such as RA/DEC, then the solving process could be directed where to start the search for matching. Since no information was directly available from the header file blind solving was required. The initial search starts very wide and could take up to 30 minutes [4] if there are very few sources in the field.

[4] The user can choose a timeout parameter to stop the process after a certain amount of time.

4.3.5 Scrape deepsky header and add WCS to aligned frames

Using Astropy's fits and WCS tools, lightcurator reads the header copies the WCS from the deepsky frame that was plate solved with Astrometer.net's service. Up to this point, the headers of all the aligned frames are blank. We attach WCS information and the keyword and value assigned to 'DATE-OBS' which is the time stamp of the observation.

4.3.6 Source Extraction

Source extraction is done with a python package called *photutils*. The steps to source extraction are as follows. First, an Astropy.stats function called *sigma_clipped_stats* takes the data frame finds the standard deviation, σ, and the median. Then, all points smaller or larger than 3σ from the median are removed or clipped. This step is done repeatedly until there are no more points beyond 3σ or 5 cycles have been completed. Lightcurator has hard-coded 3σ and the maximum iterations of 5. The function returns the calculated clipped σ, mean, and median.

From photutils, the class *DAOStarFinder* uses the DAOFIND algorithm developed by Stetson in 1987 [37]. Lightcurator hard-codes the full width half max (fwhm) at 3.0 and detection threshold at 5σ above the background. DAOFIND returns a method to find stars. The data is background subtracted before the *find_stars* method is called. The background is the median calculated in the first step. The method returns a table containing an id, xy centroid, instrumental flux, and instrumental magnitude on the stars found.

This method is applied to each aligned frame to create a catalog of sources for each frame. Lightcurator refers to these as aligned cats.

4.3.7 Extract sources from deepsky frame

The same method described in the previous section is done to the deepsky frame to create a master catalog of all possible sources detected in the frame.

4.3.8 Cross match sources from aligned frames to deepsky frame

Source cross matching is done with an Astropy package called *coordinates* using the *SkyCoord* class. The aligned catalogs are then compared to the master catalog one at a time. The SkyCoord class creates a method called *match_to_catalog_sky* which finds the nearest coordinate match between each object of the two catalogs. The matched catalog contains the same information from the sources, but only from those sources that best matched coordinates. The matched catalogs are written to file.

The final step in cross matching catalogs is to create a time series catalog that contains the id of all the sources, their fluxes, and time stamp from the observation. This is written to file and saved as an ecsv file by recommendation of Astropy documentation.

4.3.9 Cross match master catalog with other catalogs

The lightcurator function *query_from_wcs* takes a string path to a fits file with WCS. The function expects the header keywords specific to WCS information 'CRVAL1' and 'CRVAL2' for RA and DEC, respectively. Using *query_region* from the astroquery package, a search cone of 30 arc minutes is generated from a Vizier query of the following catalogs,

B/vsx AAVSO International Variable Star Index VSX [41],

B/gcvs General Catalogue of Variable Stars [34],

I/340 UCAC5 Catalogue [44],

I/345 Gaia DR2 [14].

A similar process as described in the previous section is used to match the master catalog with the Vizier query. At this point, the user can verify that the intended eclipsing binary star system is in both VSX and GCVS catalogs and that the index from both query results match with each other. The query results are used as an intermediary step, therefore only stored to memory. The reported magnitudes from UCAC and Gaia use standard filters and can be used to calibrate instrumental data.

4.3.10 Correct or normalize extracted flux data

Calibration stars are required to transform instrumental flux measurements from filtered data to a standard magnitude system. This is usually done by using cataloged magnitudes the report in a standard set of filters like Johnson UVBRI or Sloan ugriz. Since most data is unfiltered, the observations are long with changing air mass, and the field of view is small, differential photometry is used.

Differential photometry uses comparison stars to remove the effects of extinction due to changing air mass. Comparison stars are found using the following criteria,

1. the star must not be a variable star,
2. the stars must be about the same magnitude,
3. the standard deviation of the star must not be too large, and
4. the star needs to be visible for most of the observation.

Lightcurator does not yet have the tool implemented for finding comparison stars, but is under development. To meet criteria 1 a filter is generated by using the list returned from the matched sources to the VSX and GCVS catalog. Criteria 3 is met by running numpy statistics that calculate standard deviation that ignores *nan* values. Criteria 4 is met by counting the *nan* values across the time series of a single source and filtering sources with a count less than an arbitrary tolerance set at 10 percent. Criteria 4 is done by visual inspection.

The average magnitude of the comparison stars is taken for a single frame. The averaged magnitude is subtracted from the magnitude of the variable star. This is done across all frames in the time series catalog. The features due to changing air mass would appear on both variable and comparison stars. By subtracting the magnitude of the comparison star from the variable star, the variability of the star will become apparent. The difference of a non-variable star to the magnitude of the comparison will reveal a horizontal plot, if comparison stars meet the criteria.

4.3.11 Create or update database of previously observed sources

The database is not yet implemented in lightcurator, but is intended to provide magnitudes from previous observations processed by lightcurator. Tracking sources in this way will enable analysis for longer period variable stars. Future plans for lightcurator include to allow users to upload their own time series data into the database and to make a streamable service that can update the database of previously observed sources with data from new single frames to update light curves.

4.3.12 Analyzing variability

Currently, lightcurator only identifies variable stars using catalog matching with VSX and GCVS.

Immediate plans for variability analysis will be done with a python package called feets: feATURE eXTRACTOR FOR tIME sERIES, written by Cabral [5].

4.4 Eclipsing binary system modeling

PHOEBE [18, 32, 33] provides tools to create a mesh for detached, semi-detached, and contact binary stars. First, a system needs to be created that will contain all the parameters of the objects studied. Light curve data, i.e. magnitude and time, is imported to the parameter list. This step would also include importing orbital, effective temperature, and radial velocity information. When setting up the system PHOEBE automatically provides defaults to only require magnitude and time as inputs. For this process a close contact binary system is setup since the type of stars studied are EW. This means the masses of the 2 major bodies are close in mass, therefore PHEOBE defaults to 1.5 solar radii. Masses would also be calculated from radial velocities, but PHEOBE defaults to 1.0089067995 solar masses. Effective temperature requires filtered data to process so PHEOBE defaults to 6000.0 K which is in the center range of typical F-G spectral type stars that EW stars usually classify. A side by side comparison of PHEOBE parameters of SS Ari and PR Boo observations are provided in the Results chapter on figure 5.21.

CHAPTER V

RESULTS

5.1 Observed objects

From table 5.1, the following observations were processed with the lightcurator pipeline: PR Boo (figure 5.1), Ny Lyr (figure 5.3), HP Aur (figure 5.4).

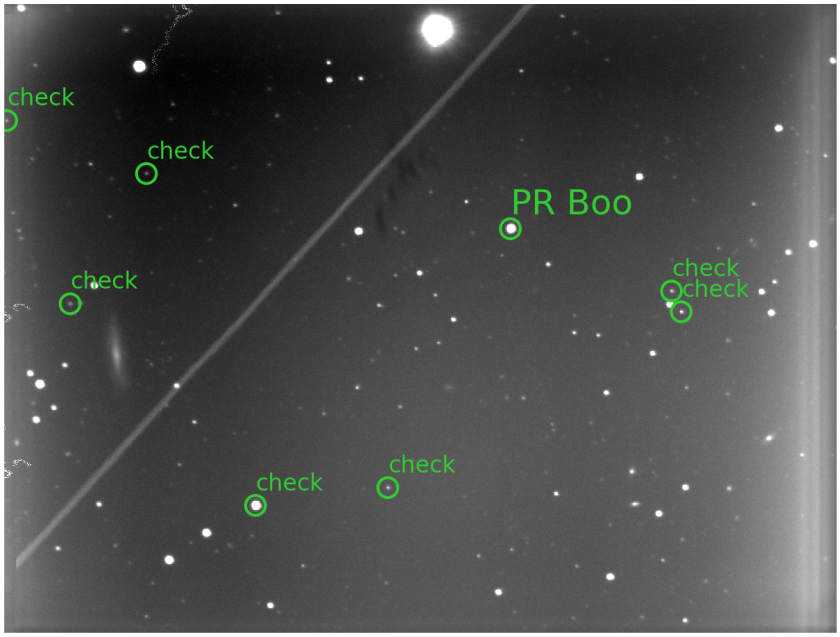

Figure 5.1: Deepsky frame of PR Boo 2017/04/20

5.1.1 Known information of targets examined

Table 5.2 are the results given by GCVS Query Form.

Target	Type	Filter	Observation date
MQ Boo	EB	C	2017/04/26
PR Boo	EW	C	2017/03/30
		C	2017/04/20
		C	2017/05/11
EQ Uma	EW/KW	CRGB	2017/04/06
HP Aur	EA	C	2017/04/13
NY Lyr	EW/KW	C	2017/07/06
AW Ari	EW	GB	2017/10/12
SS Ari	EW	C	2016/11/27
		RGB	2017/11/01
XX LMi	EW	RGB	2018/03/20
V467 Lyr	EW:/KE:	CRG	2018/06/07
V2793 Ori	EA	RGB	2017/11/17

Table 5.1: Observations of eclipsing binaries from the CTMO Data log [7]. Filters: RGB corresponds to Baader CCD RGB filters and C is unfiltered

GCVS	J2000.0	Type	Max	Min I	Min II	Period
PR Boo	151832.01 +445711.6	EW	13.44	13.85	13.79	0.3712793
NY Lyr	191636.86 +342340.5	EW/KW	12.7	13.2	13.1	0.44079534
HP Aur	051021.78 +354746.7	EA	11.16	11.79	11.55	1.4228191

Table 5.2: GCVS entries of observed eclipsing binary

5.1.2 Period analysis by feets

According to the documentation of feets, the Lomb-Scargle periodogram is optimized to identify sinusoidal-shaped periodic signals in time-series data. Since the targets are all of EW type the expected light curve should be sinusoidal. Time series data processed by lightcurator is analyzed with feets and the extracted feature is called *PeriodLS*, shown in figure 5.3

5.2 lightcurator Benchmark

Simple benchmarking was performed on two machines. Results are shown in Table 5.4.

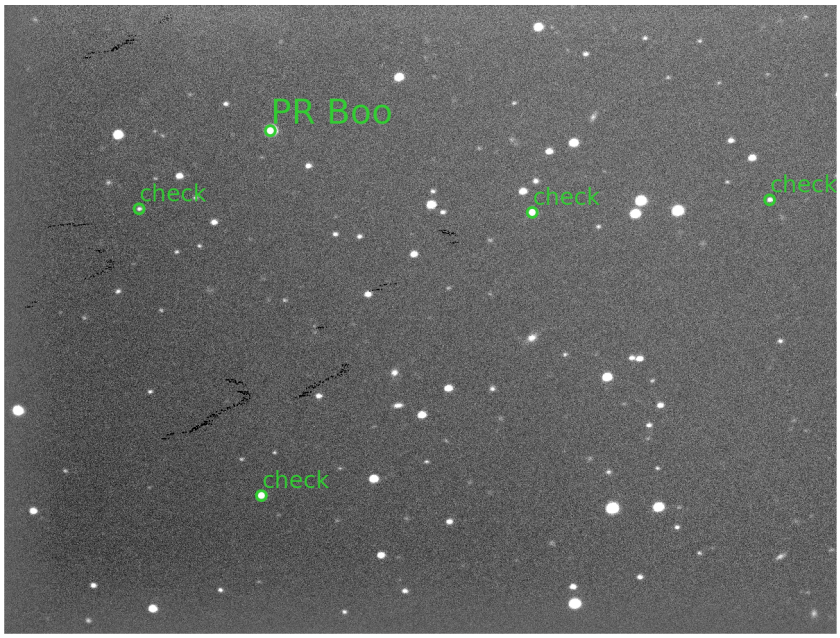

Figure 5.2: Deepsky frame of PR Boo 2017/03/30

5.2.1 Data set

Data from the observation from 2017/04/20 of PR Boo is used to perform the benchmark. The data set total size is 3.17 Gigabytes and is 746 frames of 4.1 Megabytes each.

System specifications

Operating System macOS Mojave Version 10.14.6

Object	Date	PeriodLS [d]	Period from GCVS [d]
PR Boo	2017/03/30	1.200	0.3712793
	2017/04/20	0.599	0.3712793
HP Aur	2017/04/13	0.643	1.4228191
NY Lyr	2017/07/06	2.336	0.44079534

Table 5.3: Period analysis using Lomb-Scargle method as implemented by feets

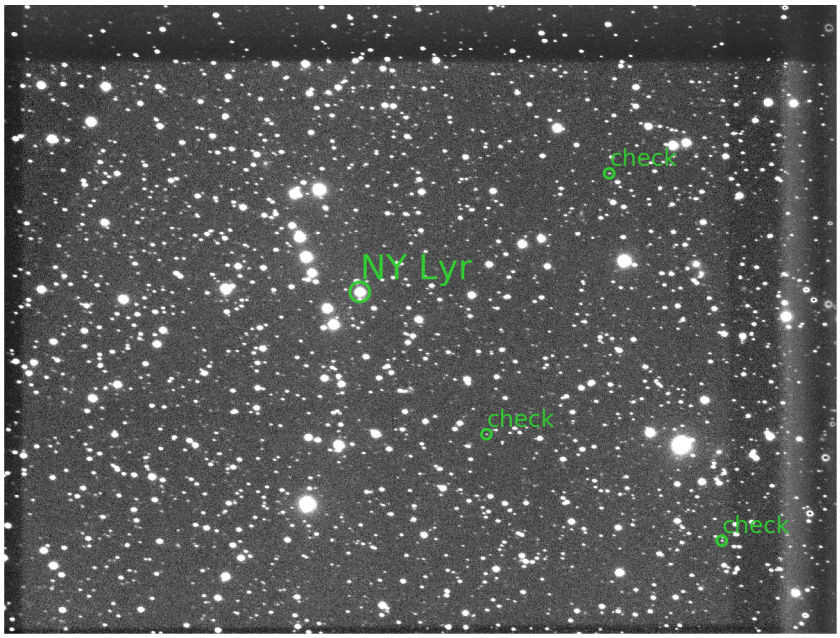

Figure 5.3: Deepsky frame of NY Lyr 2017/07/06

Processor 2.9 GHz Intel Core i5

Memory 8 GB 1867 MHz DDR3

Graphics Intel Iris Graphics 6100 1536 MB

5.3 Light curves

Light curves are generated manually from the time-series catalog generated by lightcurator.

Process type	Time to complete deepsky [s]	Total Processing time [$mm:ss$]
Serial	2659.1	57:20
Parallel	1641.2	40:26

Table 5.4: Comparison of processing types.

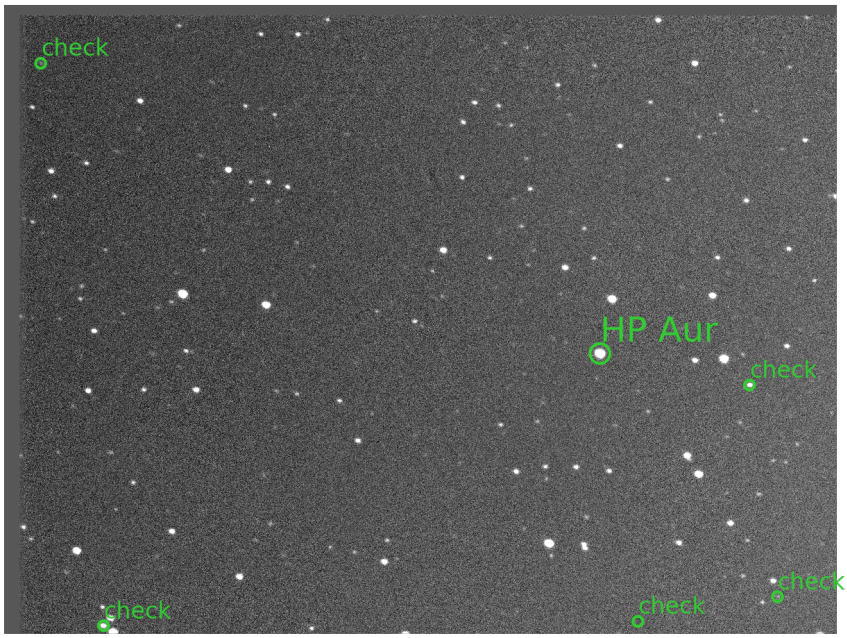

Figure 5.4: Deepsky frame of HP Aur 2017/04/14

5.3.1 PR Boo 2017/03/30

The raw data from the time-series of PR Boo is shown in figure 5.5. Magnitudes of comparison stars and their average are plotted and shown along with the variable star in figure 5.6 In figure 5.7 one comparison star is picked to compare with the averaged magnitude for comparison to show similarity in magnitude represented by a flat trend. The differential photometry light curve result is show in figure 5.8.

5.3.2 PR Boo 2017/04/20

The raw data from the time-series of PR Boo is shown in figure 5.9. Magnitudes of comparison stars and their average are plotted and shown along with the variable star in figure 5.10 In figure 5.11 one comparison star is picked to compare with the averaged magnitude for comparison to show similarity in magnitude represented by a flat trend. The differential photometry light

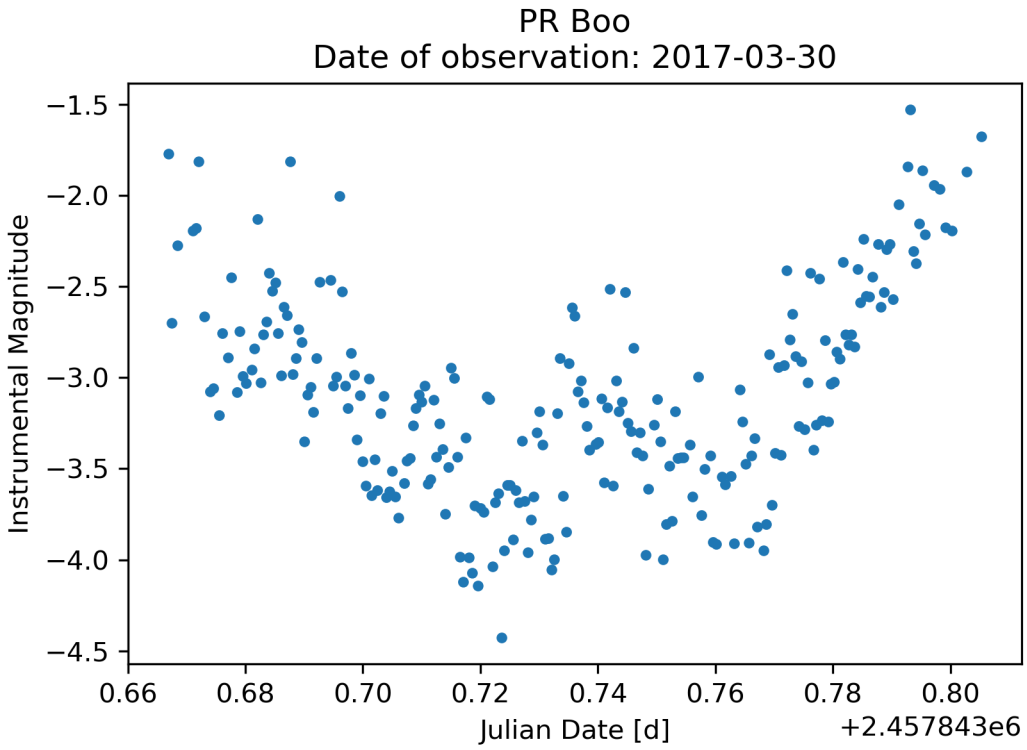

Figure 5.5: Light curve of PR Boo before differential photometry.

curve result is show in figure 5.12.

5.3.3 HP Aur 2017/04/13

The raw data from the time-series of HP Aur is shown in figure 5.13. Magnitudes of comparison stars and their average are plotted and shown along with the variable star in figure 5.14 In figure 5.15 one comparison star is picked to compare with the averaged magnitude for comparison to show similarity in magnitude represented by a flat trend. The differential photometry light curve result is show in figure 5.16.

5.3.4 NY Lyr 2017/07/06

The raw data from the time-series of NY Lyr is shown in figure 5.17. Magnitudes of comparison stars and their average are plotted and shown along with the variable star in figure 5.18 In figure 5.19 one comparison star is picked to compare with the averaged magnitude for comparison to show similarity in magnitude represented by a flat trend. The differential photometry light

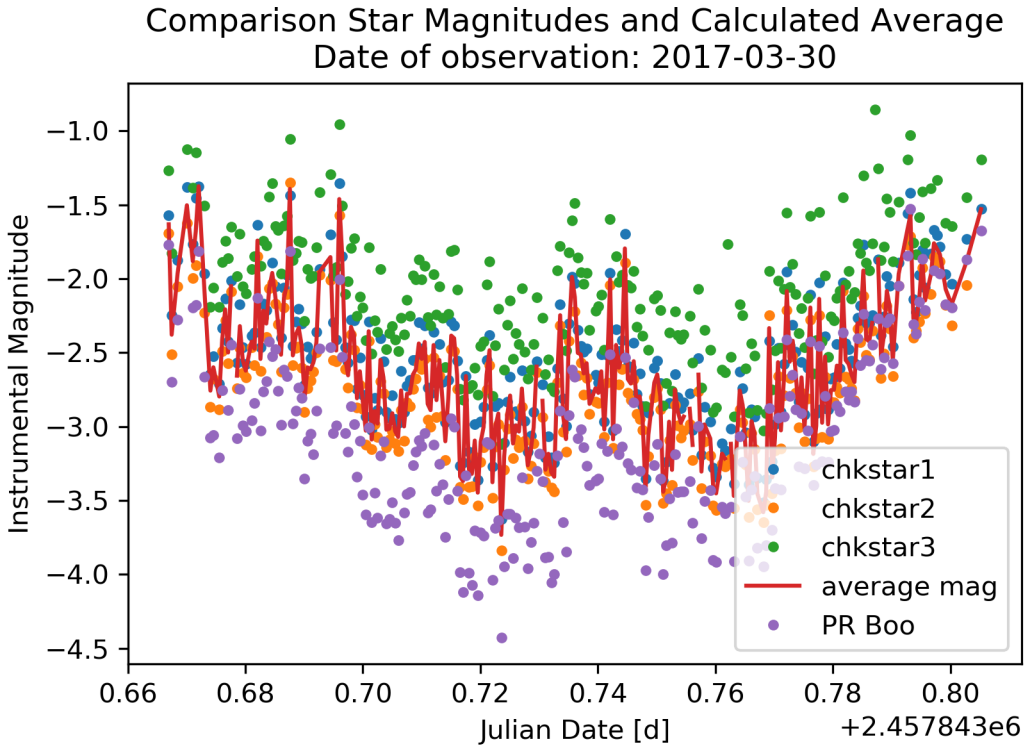

Figure 5.6: Light curve of comparison stars, averaged magnitude for comparison, and PR Boo.

curve result is show in figure 5.20.

5.4 Eclipsing binary modeling

Results of the modeling of the eclipsing binary system of PR Boo is shown on figure 5.22. A comparison of SS Ari and PR Boo parameters are shown on figure 5.21.

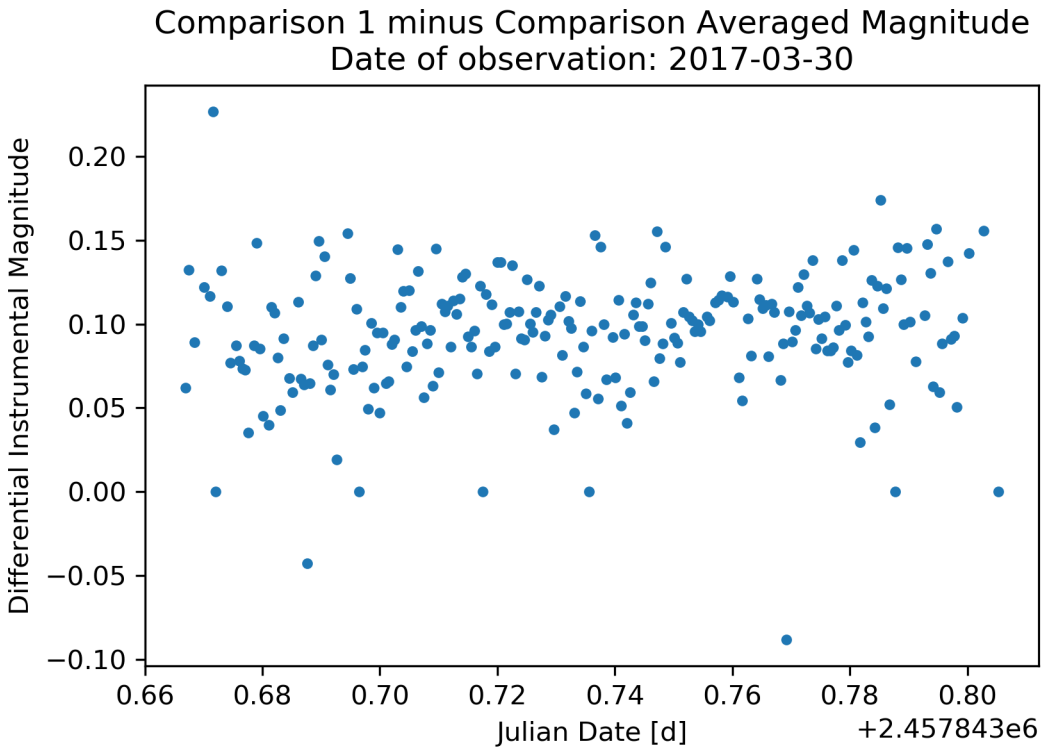

Figure 5.7: Difference between comparison star 1 and averaged magnitude for comparison.

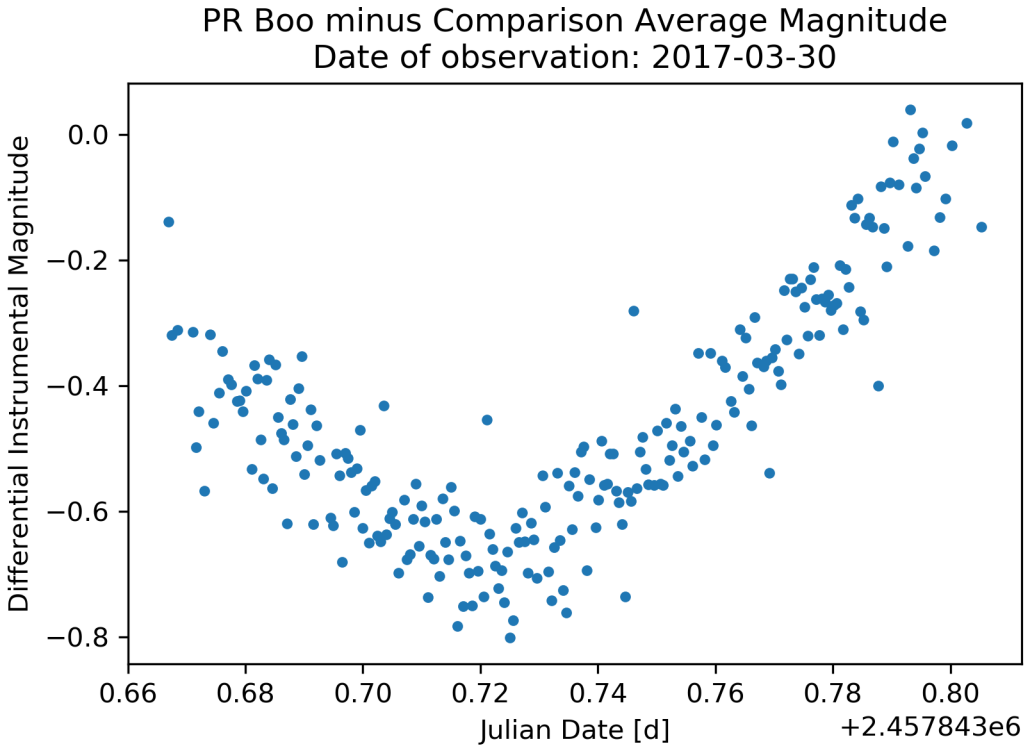

Figure 5.8: Differential photometry of PR Boo.

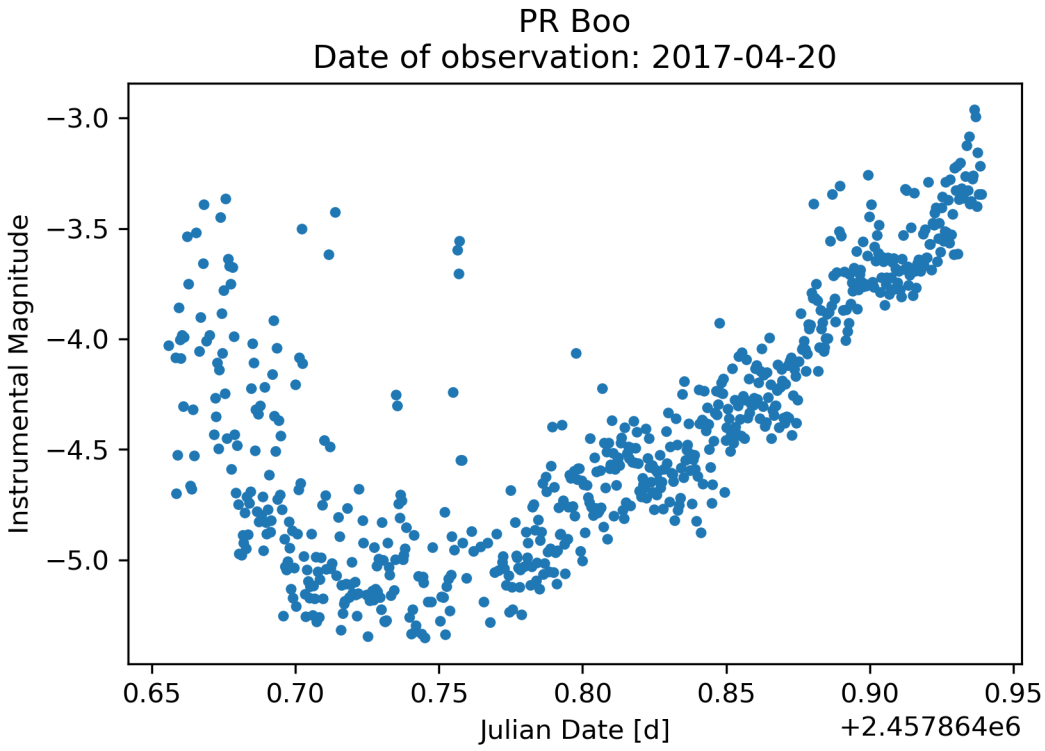

Figure 5.9: Light curve of PR Boo before differential photometry.

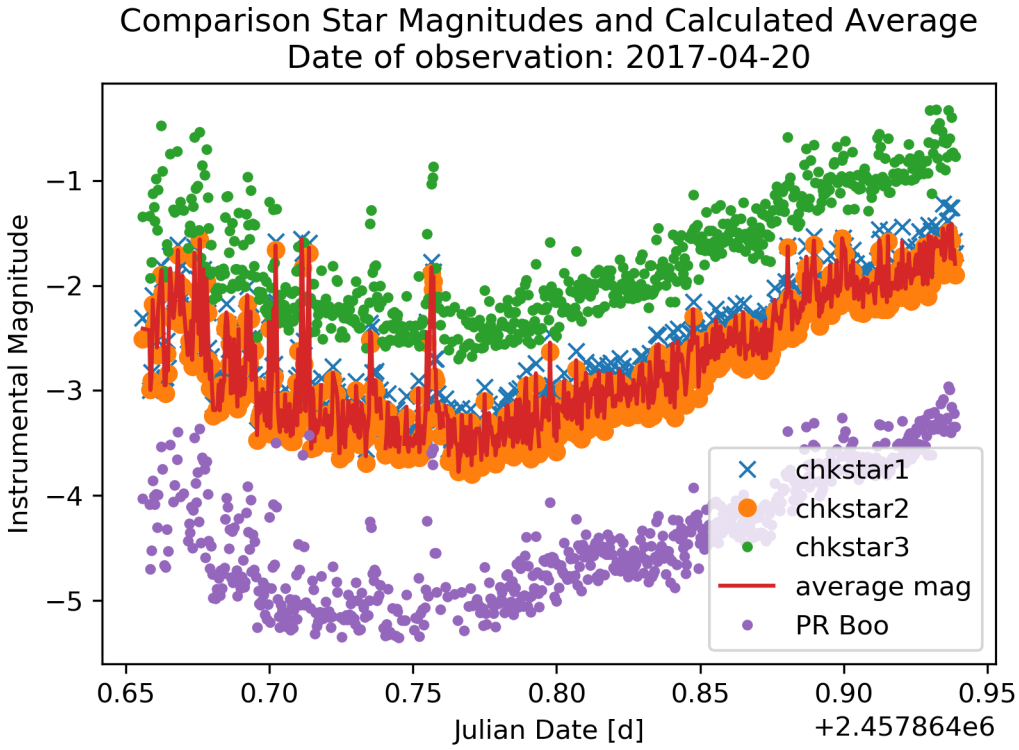

Figure 5.10: Light curve of comparison stars, averaged magnitude for comparison, and PR Boo.

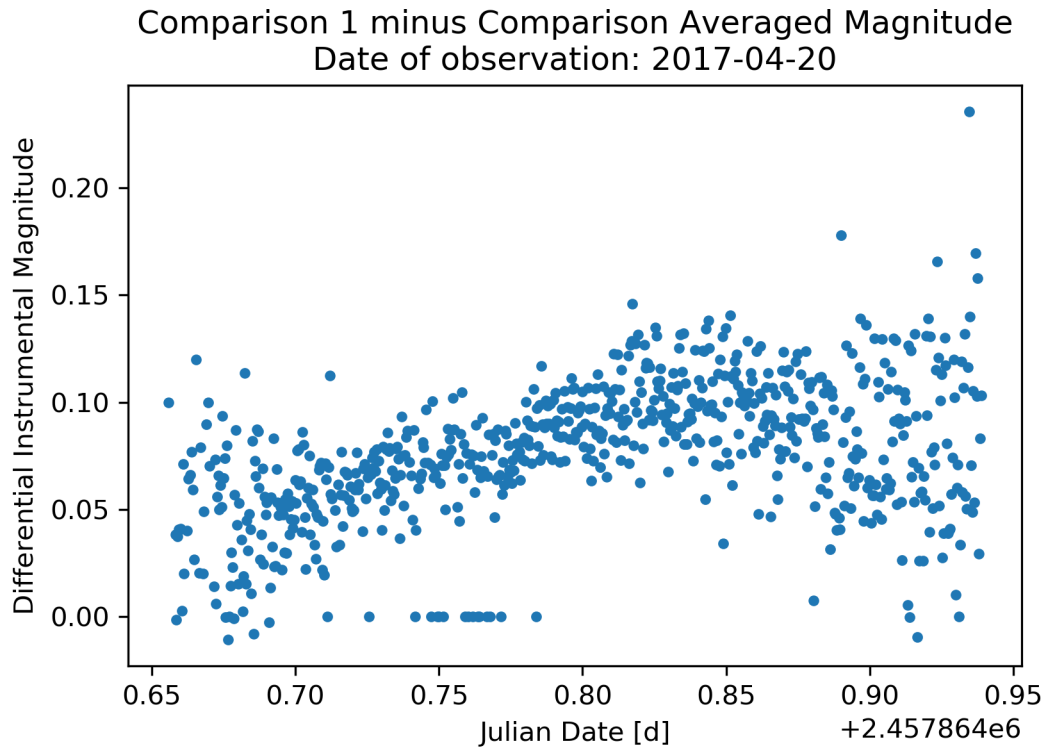

Figure 5.11: Difference between comparison star 1 and averaged magnitude for comparison.

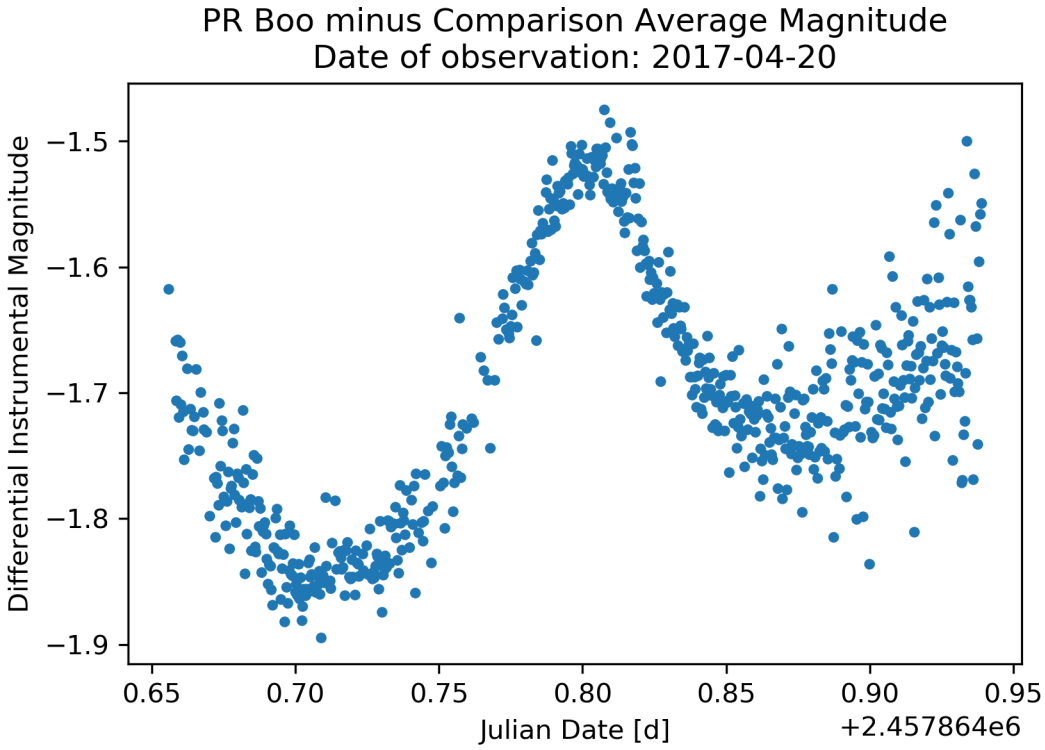

Figure 5.12: Differential photometry of PR Boo.

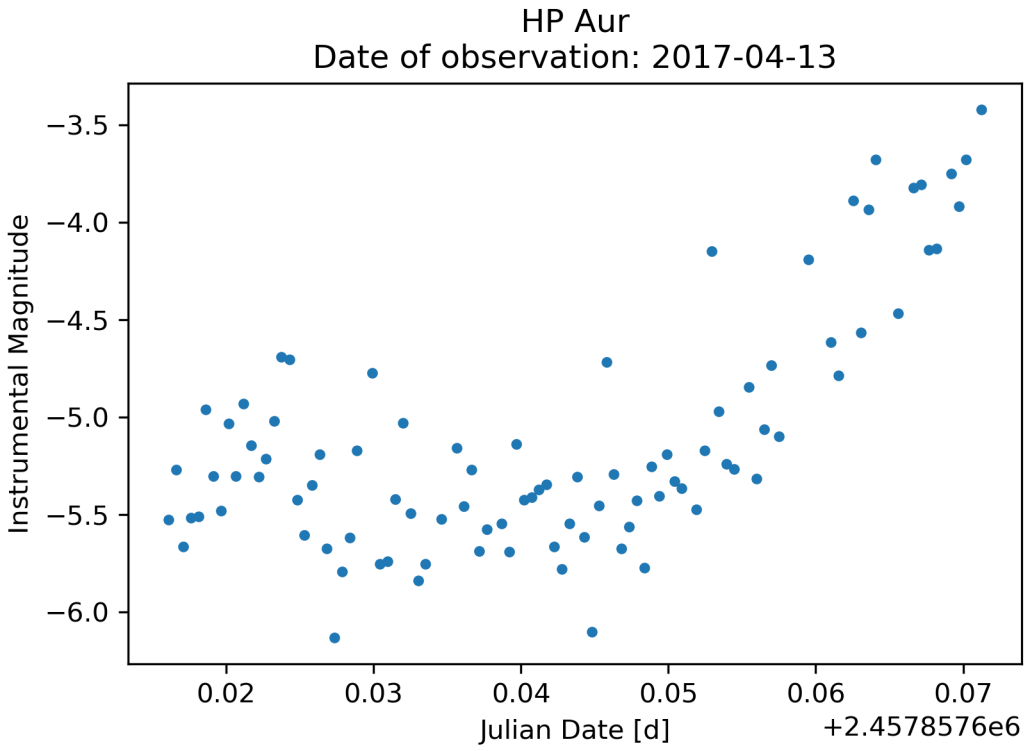

Figure 5.13: Light curve of HP Aur before differential photometry.

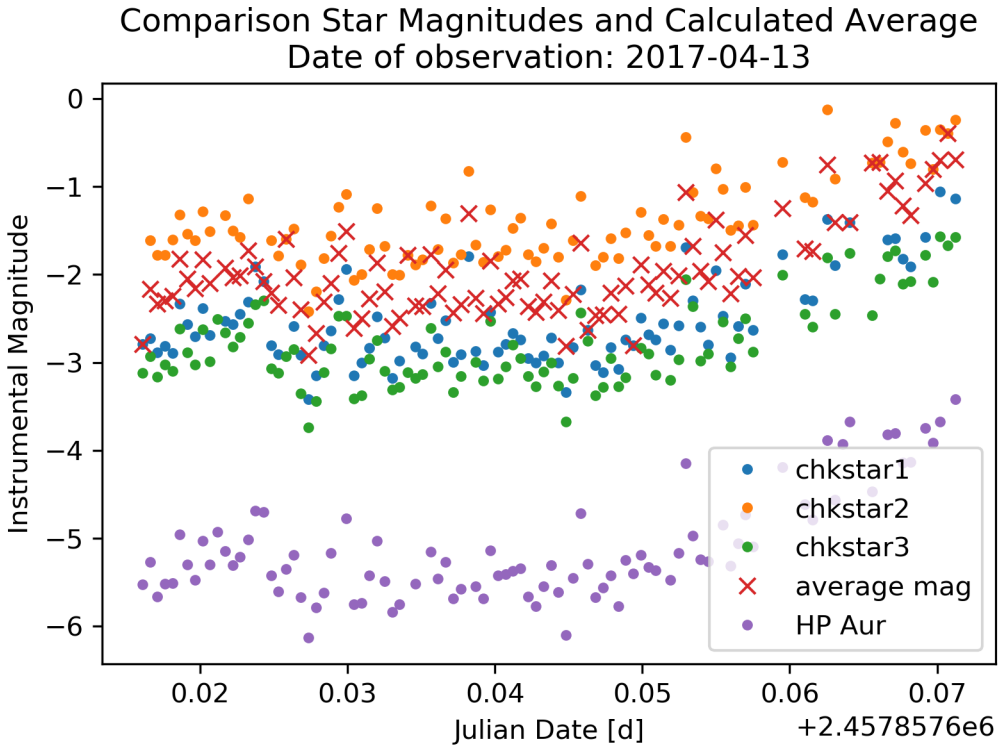

Figure 5.14: Light curve of comparison stars, averaged magnitude for comparison, and HP Aur.

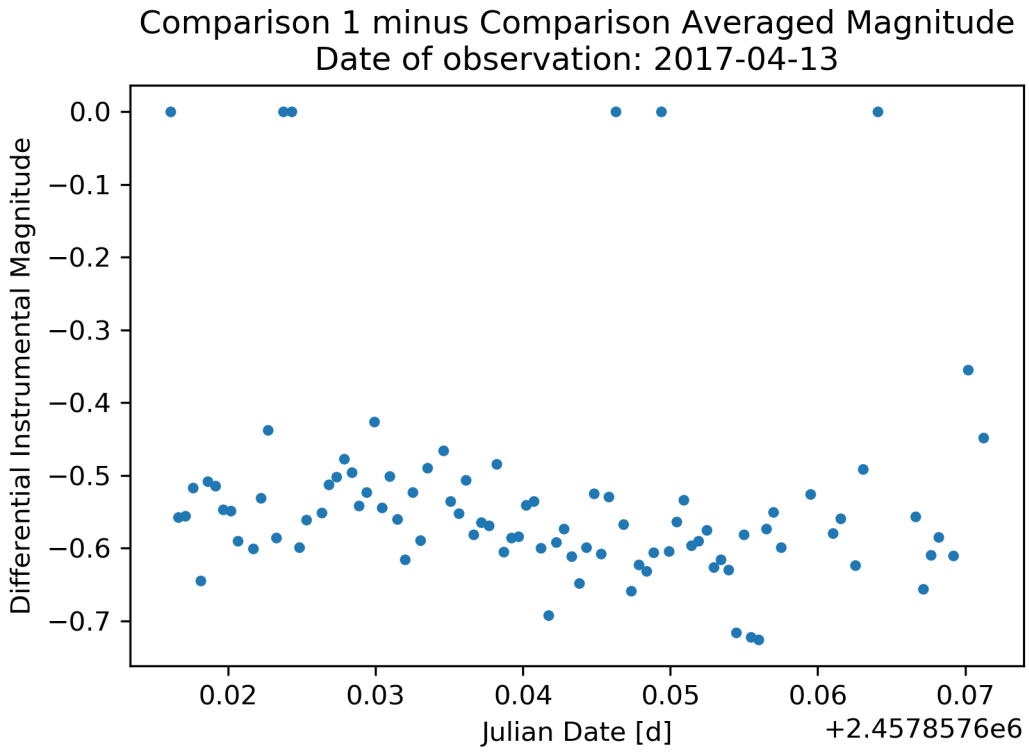

Figure 5.15: Difference between comparison star 1 and averaged magnitude for comparison.

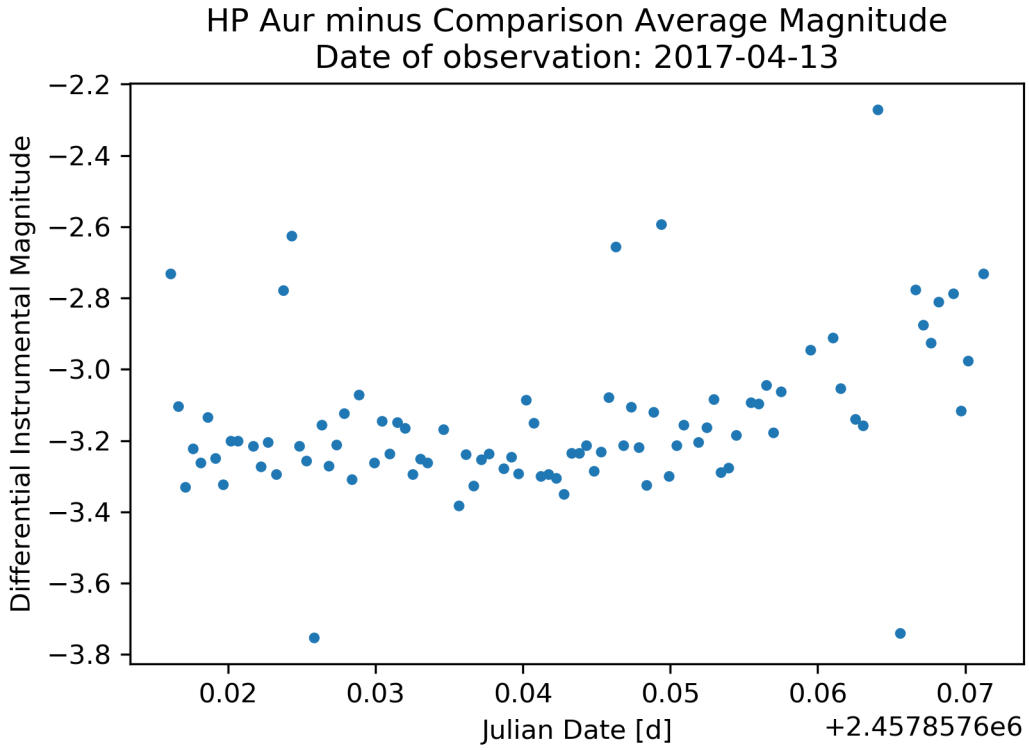

Figure 5.16: Differential photometry of HP Aur.

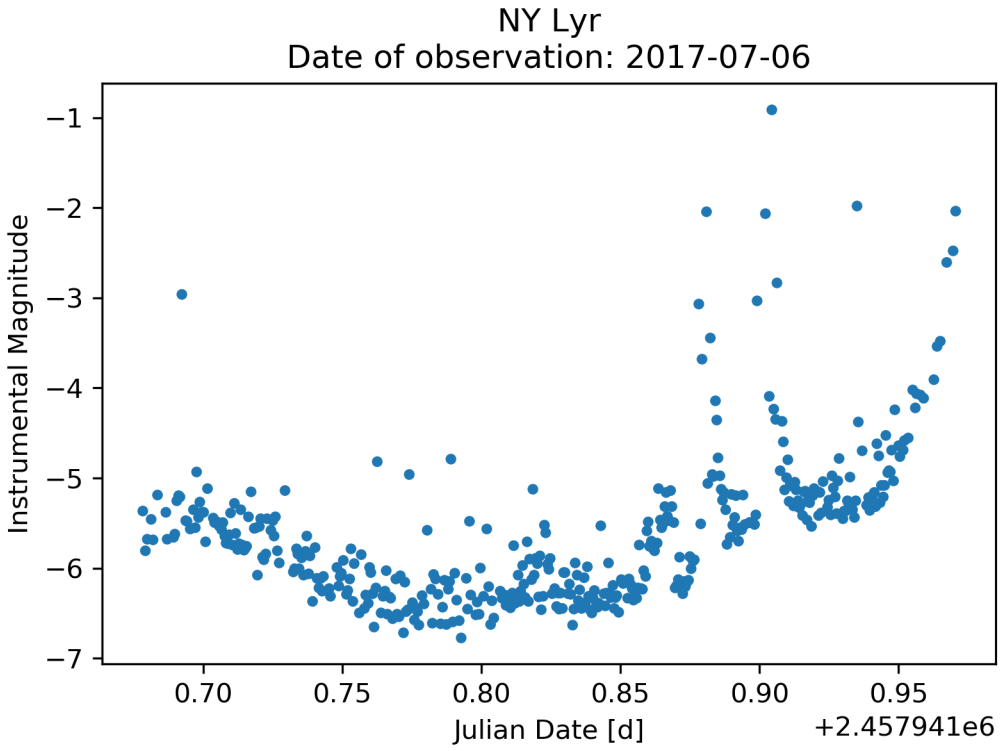

Figure 5.17: Light curve of NY Lyr before differential photometry.

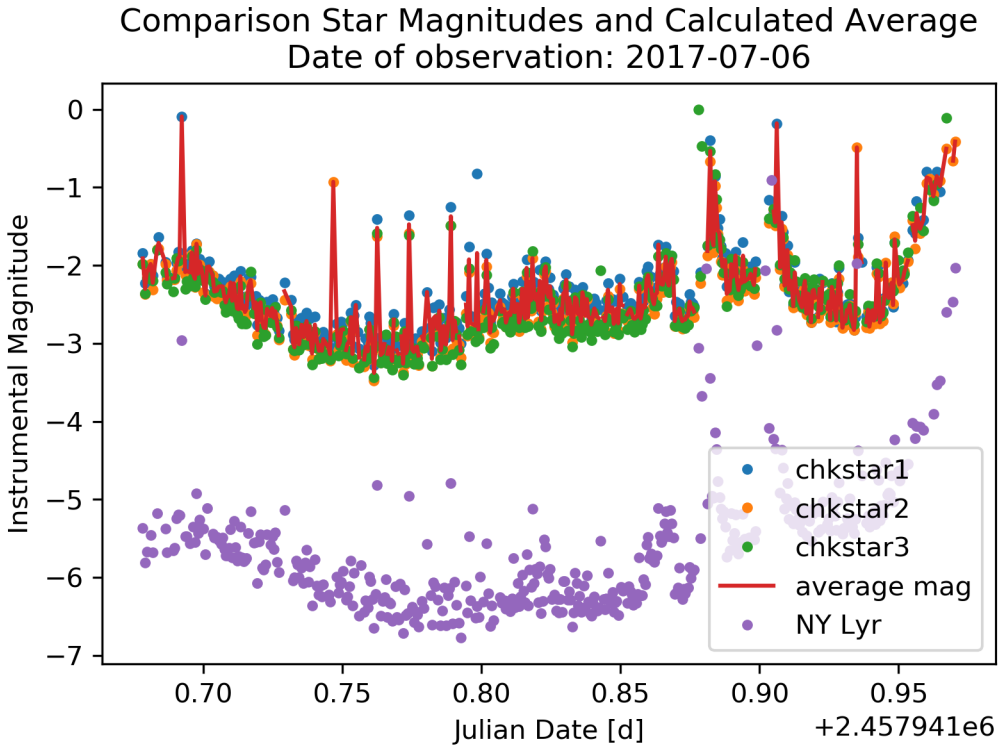

Figure 5.18: Light curve of comparison stars, averaged magnitude for comparison, and NY Lyr.

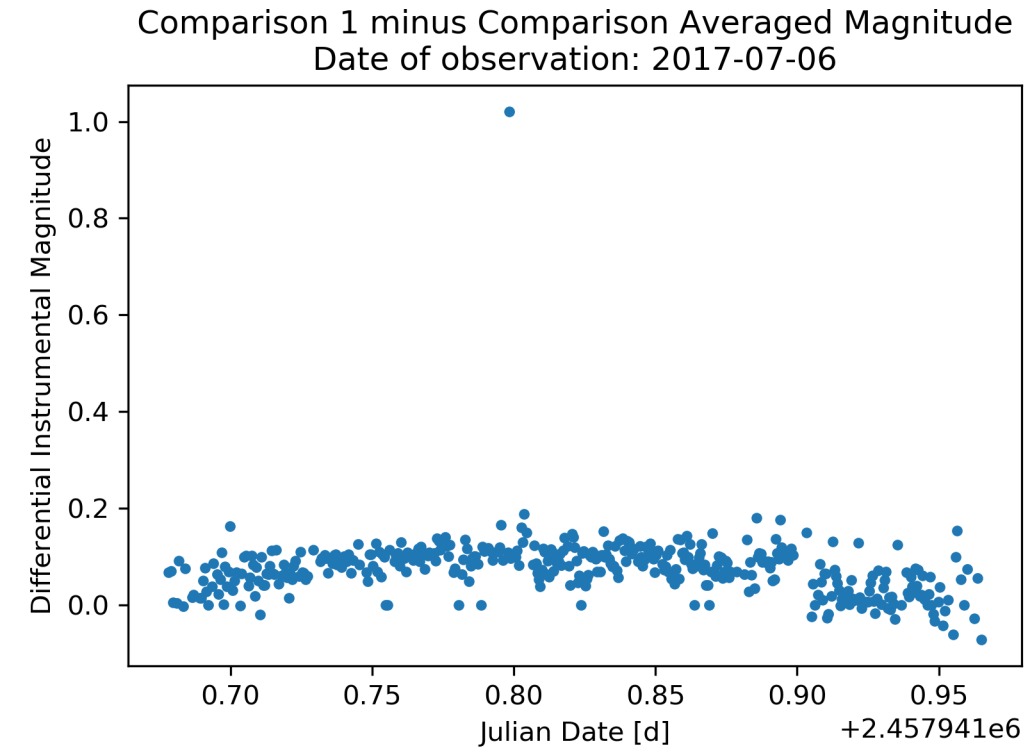

Figure 5.19: Difference between comparison star 1 and averaged magnitude for comparison.

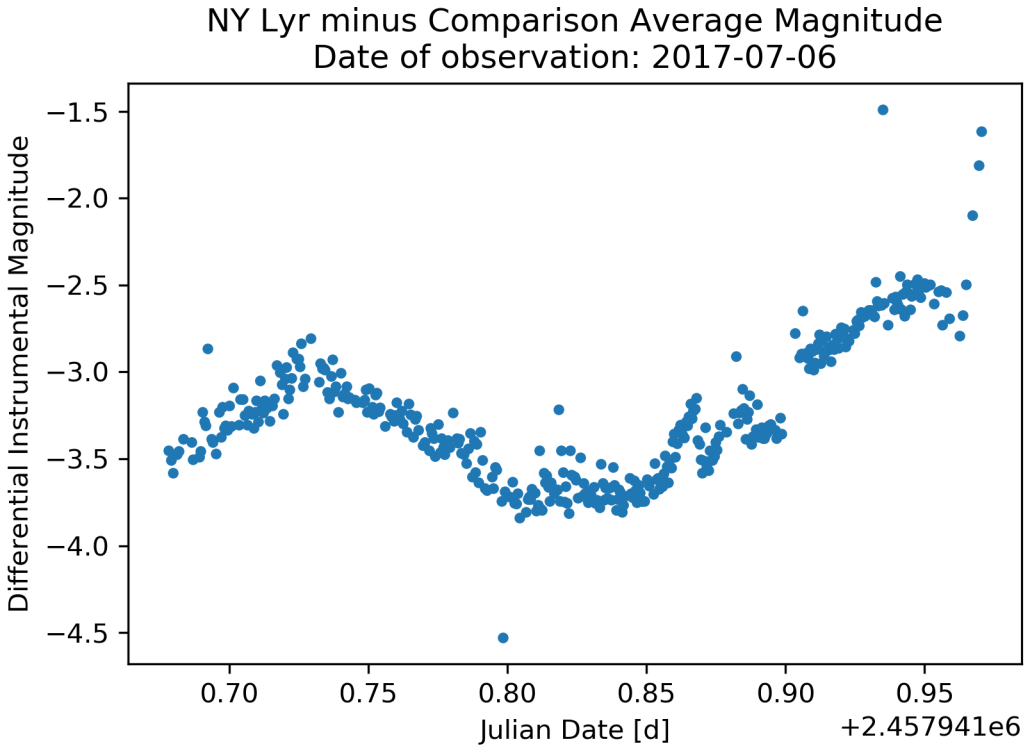

Figure 5.20: Differential photometry of NY Lyr.

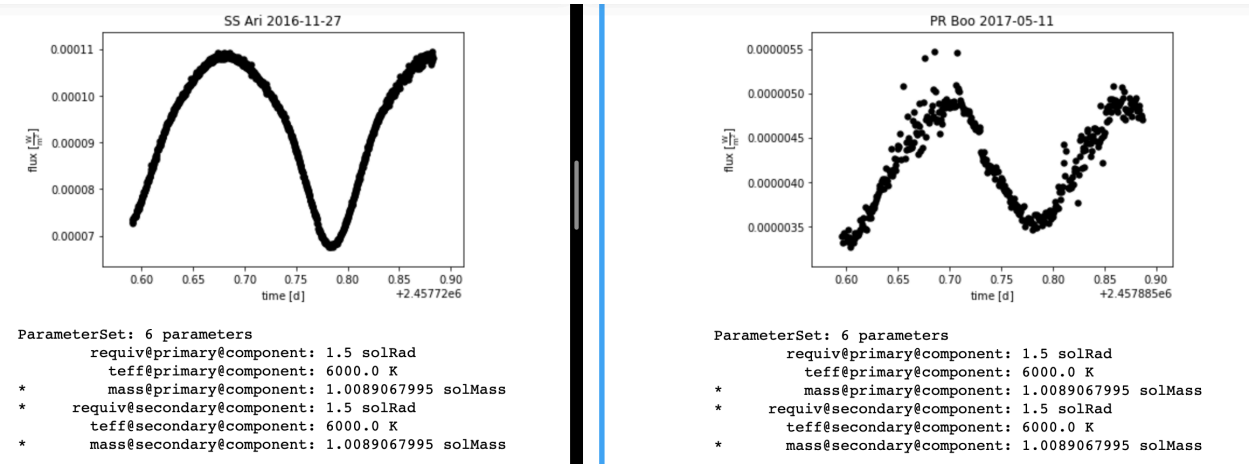

Figure 5.21: Side by side comparison of SS Ari and PR Boo light curve parameters given by PHEOBE.

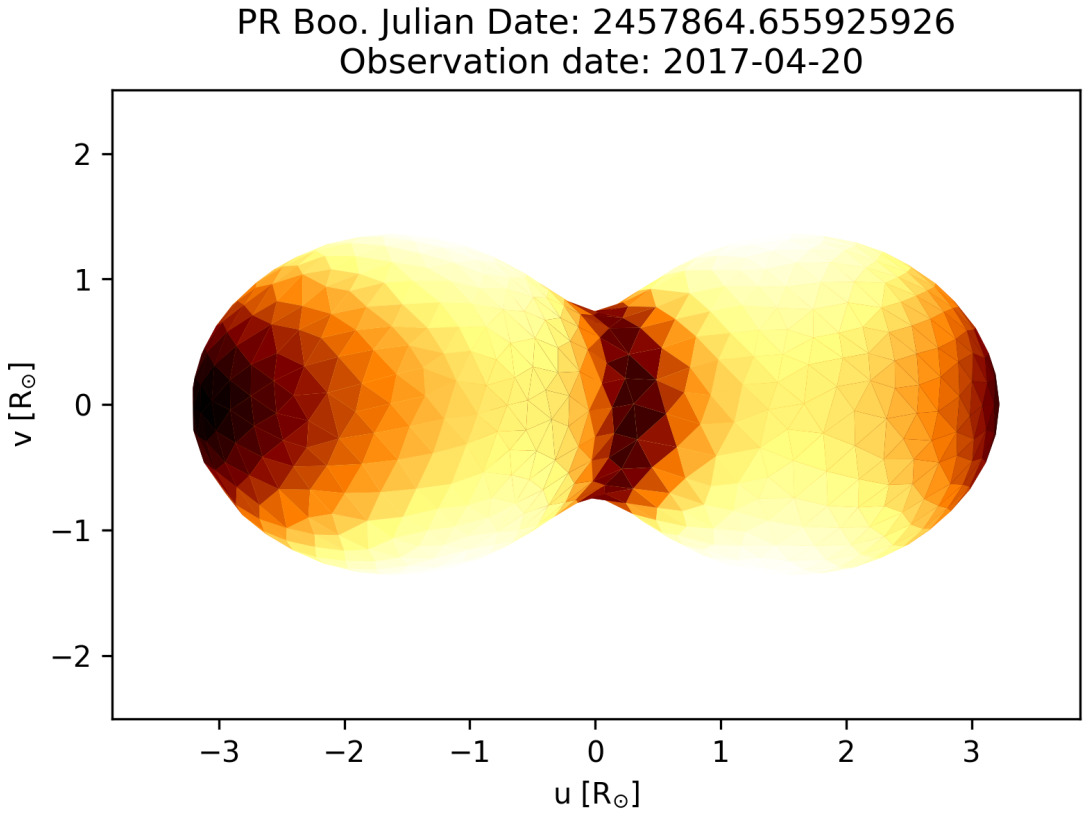

Figure 5.22: Model of eclipsing binary system PR Boo generated by PHOEBE.

CHAPTER VI

CONCLUSION

6.1 Variable star detection

Eclipsing binary star detection by cross identification with VSX and GCVS was successful in all 5 data sets observed. Other variable stars including other eclipsing binaries were detected in the same field as the original intended targets of observation. Once the implementation of a database is complete then the extractors available on feets can analyze and rank variability.

6.2 Eclipsing binary characterization

Only period was calculated using the Lomb-Scargle Method for finding period. HP Aur has a much longer period than was actually observed, therefore it is expected that period analysis will result in poor relation to the period reported by GCVS. Between the two observations of PR Boo only one had a complete period that resulted in a closer match to the reported period on GCVS. The large discrepancy between the periods of NY Lyr are most likely effects due to the single aperture that was selected based on average seeing. The reported maximum magnitude of 11.16 for NY Lyr suggests that a different aperture should be used.

6.2.1 Limitations on characterization

CTMO is being upgraded to include a spectrometer for spectral data collection. Radial velocities cannot be measured without spectral data. For this reason eclipsing binary system mass calculations cannot be achieved at CTMO. At least 2 filters are required for effective temperature calculations. Since most data taken from the first years of CTMO is unfiltered effective temperatures cannot be calculated.

6.3 Considerations for the future

Aperture photometry relies on selecting appropriate aperture size for a given observation. This can be systematically found by calculating the full width half maximum of a source to determine the radius of aperture in pixels. Point spread function (PSF) photometry is a better approximation of a profile of a source taking into account the more Gaussian-like distribution of signal across the pixels of a CCD. Currently, photutils v0.6 has a PSF Photometry module that is considered experimental and not used for this reason.

Lightcurator relies on Astrometry.net service for attaching WCS and assumes this step must be completed. To make lightcurator more universal, this step must be made optional. Since Astrometry.net is not a python package the user must install the Astrometry program. The image registration software, astroalign, has the potential to attach WCS if using one reference image with proper WCS, thus eliminating the need for software outside the python environment. Astroalign does not currently have this feature.

Optimization can be performed by reducing the number of times a file is saved to memory to read the header. Statistics of every data frame is performed on multiple occasions as part of intermediary steps such as source detection for image registration. Lightcurator could switch the order of the pipeline and get xy source positions and flux measurements first. Then by using the xy pixel positions from the data frames in astroalign the source matching can be done without the need for running source extraction. Benchmarking of both methods will need to be performed for comparison.

Lastly, for proper long term period analysis transformations to a standard system should be performed. As a first order approximation for unfiltered data comparison star magnitudes using the reported Johnson V magnitude are typically used. Given that lightcurator already can query VizieR Catalogs this upgrade should be possible.

BIBLIOGRAPHY

[1] ANDOR. *Apogee Alta F16 Specification Sheet*. ANDOR, 2019.

[2] Astropy Collaboration, T. P. Robitaille, E. J. Tollerud, P. Greenfield, M. Droettboom, E. Bray, T. Aldcroft, M. Davis, A. Ginsburg, A. M. Price-Whelan, W. E. Kerzendorf, A. Conley, N. Crighton, K. Barbary, D. Muna, H. Ferguson, F. Grollier, M. M. Parikh, P. H. Nair, H. M. Unther, C. Deil, J. Woillez, S. Conseil, R. Kramer, J. E. H. Turner, L. Singer, R. Fox, B. A. Weaver, V. Zabalza, Z. I. Edwards, K. Azalee Bostroem, D. J. Burke, A. R. Casey, S. M. Crawford, N. Dencheva, J. Ely, T. Jenness, K. Labrie, P. L. Lim, F. Pierfederici, A. Pontzen, A. Ptak, B. Refsdal, M. Servillat, and O. Streicher. Astropy: A community Python package for astronomy. A&A, 558:A33, October 2013. doi: 10.1051/0004-6361/201322068.

[3] Martin Beroiz. toros-astro/astroalign: Release Candidate 1 for Version 2.0, May 2019. URL `https://doi.org/10.5281/zenodo.3234002`.

[4] Larry Bradley, Brigitta Sipocz, Thomas Robitaille, Erik Tollerud, Zé Vinícius, Christoph Deil, Kyle Barbary, Hans Moritz Günther, Mihai Cara, Ivo Busko, Simon Conseil, Michael Droettboom, Azalee Bostroem, E. M. Bray, Lars Andersen Bratholm, Tom Wilson, Matt Craig, Geert Barentsen, Sergio Pascual, Axel Donath, Johnny Greco, Gabriel Perren, P. L. Lim, and Wolfgang Kerzendorf. astropy/photutils: v0.6, January 2019. URL `https://doi.org/10.5281/zenodo.2533376`.

[5] JB Cabral, B Sánchez, F Ramos, S Gurovich, P Granitto, and J Vanderplas. From fats to feets: Further improvements to an astronomical feature extraction tool based on machine learning. *Astronomy and Computing*, 2018.

[6] Richard Camuccio. CCD Analysis. 2019.

[7] Richard Camuccio. CTMO Data Log. 2019.

[8] Moises Castillo. moemyself3/lightcurator: Alpha revision 4 for Version 1.0, August 2019. URL https://doi.org/10.5281/zenodo.3358197.

[9] Patrick Chevalley. Cartes du ciel-skychart, 2006. URL https://www.ap-i.net/skychart/en/start.

[10] Frederick R. Chromey. *To Measure the Sky*. 2010.

[11] Meade Instruments Corporation. *8", 10", 12", 14", 16" LX200GPS Schmidt-Cassegrain Telescopes 7" LX200GPS Maksutov-Cassegrain Telescope with Autostar II Hand Controller*. Meade Instruments Corporation, 2003.

[12] Matt Craig, Steve Crawford, Michael Seifert, Thomas Robitaille, Brigitta Sipőcz, Josh Walawender, Zè Vinícius, Joe Philip Ninan, Michael Droettboom, Jiyong Youn, Erik Tollerud, Erik Bray, Nathan Walker, VSN Reddy Janga, Connor Stotts, Hans Moritz Günther, Evert Rol, Yoonsoo P. Bach, Larry Bradley, Christoph Deil, Adrian Price-Whelan, Kyle Barbary, Anthony Horton, William Schoenell, Nathan Heidt, Forrest Gasdia, Stefan Nelson, and Ole Streicher. astropy/ccdproc: v1.3.0.post1, December 2017. URL https://doi.org/10.5281/zenodo.1069648.

[13] Diffraction Limited. Cyanogen imaging maxim dl, 1997. URL https://diffractionlimited.com/product/maxim-dl/.

[14] Gaia Collaboration, A. G. A. Brown, A. Vallenari, T. Prusti, J. H. J. de Bruijne, C. Babusiaux, C. A. L. Bailer-Jones, M. Biermann, D. W. Evans, L. Eyer, F. Jansen, C. Jordi, S. A. Klioner, U. Lammers, L. Lindegren, X. Luri, F. Mignard, C. Panem, D. Pourbaix, S. Randich, P. Sartoretti, H. I. Siddiqui, C. Soubiran, F. van Leeuwen, N. A. Walton, F. Arenou, U. Bastian, M. Cropper, R. Drimmel, D. Katz, M. G. Lattanzi, J. Bakker,

C. Cacciari, J. Castañeda, L. Chaoul, N. Cheek, F. De Angeli, C. Fabricius, R. Guerra, B. Holl, E. Masana, R. Messineo, N. Mowlavi, K. Nienartowicz, P. Panuzzo, J. Portell, M. Riello, G. M. Seabroke, P. Tanga, F. Thévenin, G. Gracia-Abril, G. Comoretto, M. Garcia-Reinaldos, D. Teyssier, M. Altmann, R. Andrae, M. Audard, I. Bellas-Velidis, K. Benson, J. Berthier, R. Blomme, P. Burgess, G. Busso, B. Carry, A. Cellino, G. Clementini, M. Clotet, O. Creevey, M. Davidson, J. De Ridder, L. Delchambre, A. Dell'Oro, C. Ducourant, J. Fernández-Hernández, M. Fouesneau, Y. Frémat, L. Galluccio, M. García-Torres, J. González-Núñez, J. J. González-Vidal, E. Gosset, L. P. Guy, J. L. Halbwachs, N. C. Hambly, D. L. Harrison, J. Hernández, D. Hestroffer, S. T. Hodgkin, A. Hutton, G. Jasniewicz, A. Jean-Antoine-Piccolo, S. Jordan, A. J. Korn, A. Krone-Martins, A. C. Lanzafame, T. Lebzelter, W. Löffler, M. Manteiga, P. M. Marrese, J. M. Martín-Fleitas, A. Moitinho, A. Mora, K. Muinonen, J. Osinde, E. Pancino, T. Pauwels, J. M. Petit, A. Recio-Blanco, P. J. Richards, L. Rimoldini, A. C. Robin, L. M. Sarro, C. Siopis, M. Smith, A. Sozzetti, M. Süveges, J. Torra, W. van Reeven, U. Abbas, A. Abreu Aramburu, S. Accart, C. Aerts, G. Altavilla, M. A. Álvarez, R. Alvarez, J. Alves, R. I. Anderson, A. H. Andrei, E. Anglada Varela, E. Antiche, T. Antoja, B. Arcay, T. L. Astraatmadja, N. Bach, S. G. Baker, L. Balaguer-Núñez, P. Balm, C. Barache, C. Barata, D. Barbato, F. Barblan, P. S. Barklem, D. Barrado, M. Barros, M. A. Barstow, S. Bartholomé Muñoz, J. L. Bassilana, U. Becciani, M. Bellazzini, A. Berihuete, S. Bertone, L. Bianchi, O. Bienaymé, S. Blanco-Cuaresma, T. Boch, C. Boeche, A. Bombrun, R. Borrachero, D. Bossini, S. Bouquillon, G. Bourda, A. Bragaglia, L. Bramante, M. A. Breddels, A. Bressan, N. Brouillet, T. Brüsemeister, E. Brugaletta, B. Bucciarelli, A. Burlacu, D. Busonero, A. G. Butkevich, R. Buzzi, E. Caffau, R. Cancelliere, G. Cannizzaro, T. Cantat-Gaudin, R. Carballo, T. Carlucci, J. M. Carrasco, L. Casamiquela, M. Castellani, A. Castro-Ginard, P. Charlot, L. Chemin, A. Chiavassa, G. Cocozza, G. Costigan, S. Cowell, F. Crifo, M. Crosta, C. Crowley, J. Cuypers, C. Dafonte, Y. Damerdji, A. Dapergolas, P. David, M. David, P. de Lav-

erny, F. De Luise, R. De March, D. de Martino, R. de Souza, A. de Torres, J. Debosscher, E. del Pozo, M. Delbo, A. Delgado, H. E. Delgado, P. Di Matteo, S. Diakite, C. Diener, E. Distefano, C. Dolding, P. Drazinos, J. Durán, B. Edvardsson, H. Enke, K. Eriksson, P. Esquej, G. Eynard Bontemps, C. Fabre, M. Fabrizio, S. Faigler, A. J. Falcão, M. Farràs Casas, L. Federici, G. Fedorets, P. Fernique, F. Figueras, F. Filippi, K. Findeisen, A. Fonti, E. Fraile, M. Fraser, B. Frézouls, M. Gai, S. Galleti, D. Garabato, F. García-Sedano, A. Garofalo, N. Garralda, A. Gavel, P. Gavras, J. Gerssen, R. Geyer, P. Giacobbe, G. Gilmore, S. Girona, G. Giuffrida, F. Glass, M. Gomes, M. Granvik, A. Gueguen, A. Guerrier, J. Guiraud, R. Gutiérrez-Sánchez, R. Haigron, D. Hatzidimitriou, M. Hauser, M. Haywood, U. Heiter, A. Helmi, J. Heu, T. Hilger, D. Hobbs, W. Hofmann, G. Holland, H. E. Huckle, A. Hypki, V. Icardi, K. Janßen, G. Jevardat de Fombelle, P. G. Jonker, Á. L. Juhász, F. Julbe, A. Karampelas, A. Kewley, J. Klar, A. Kochoska, R. Kohley, K. Kolenberg, M. Kontizas, E. Kontizas, S. E. Koposov, G. Kordopatis, Z. Kostrzewa-Rutkowska, P. Koubsky, S. Lambert, A. F. Lanza, Y. Lasne, J. B. Lavigne, Y. Le Fustec, C. Le Poncin-Lafitte, Y. Lebreton, S. Leccia, N. Leclerc, I. Lecoeur-Taibi, H. Lenhardt, F. Leroux, S. Liao, E. Licata, H. E. P. Lindstrøm, T. A. Lister, E. Livanou, A. Lobel, M. López, S. Managau, R. G. Mann, G. Mantelet, O. Marchal, J. M. Marchant, M. Marconi, S. Marinoni, G. Marschalkó, D. J. Marshall, M. Martino, G. Marton, N. Mary, D. Massari, G. Matijevič, T. Mazeh, P. J. McMillan, S. Messina, D. Michalik, N. R. Millar, D. Molina, R. Molinaro, L. Molnár, P. Montegriffo, R. Mor, R. Morbidelli, T. Morel, D. Morris, A. F. Mulone, T. Muraveva, I. Musella, G. Nelemans, L. Nicastro, L. Noval, W. O'Mullane, C. Ordénovic, D. Ordóñez-Blanco, P. Osborne, C. Pagani, I. Pagano, F. Pailler, H. Palacin, L. Palaversa, A. Panahi, M. Pawlak, A. M. Piersimoni, F. X. Pineau, E. Plachy, G. Plum, E. Poggio, E. Poujoulet, A. Prša, L. Pulone, E. Racero, S. Ragaini, N. Rambaux, M. Ramos-Lerate, S. Regibo, C. Reylé, F. Riclet, V. Ripepi, A. Riva, A. Rivard, G. Rixon, T. Roegiers, M. Roelens, M. Romero-Gómez, N. Rowell, F. Royer,

L. Ruiz-Dern, G. Sadowski, T. Sagristà Sellés, J. Sahlmann, J. Salgado, E. Salguero, N. Sanna, T. Santana-Ros, M. Sarasso, H. Savietto, M. Schultheis, E. Sciacca, M. Segol, J. C. Segovia, D. Ségransan, I. C. Shih, L. Siltala, A. F. Silva, R. L. Smart, K. W. Smith, E. Solano, F. Solitro, R. Sordo, S. Soria Nieto, J. Souchay, A. Spagna, F. Spoto, U. Stampa, I. A. Steele, H. Steidelmüller, C. A. Stephenson, H. Stoev, F. F. Suess, J. Surdej, L. Szabados, E. Szegedi-Elek, D. Tapiador, F. Taris, G. Tauran, M. B. Taylor, R. Teixeira, D. Terrett, P. Teyssand ier, W. Thuillot, A. Titarenko, F. Torra Clotet, C. Turon, A. Ulla, E. Utrilla, S. Uzzi, M. Vaillant, G. Valentini, V. Valette, A. van Elteren, E. Van Hemelryck, M. van Leeuwen, M. Vaschetto, A. Vecchiato, J. Veljanoski, Y. Viala, D. Vicente, S. Vogt, C. von Essen, H. Voss, V. Votruba, S. Voutsinas, G. Walmsley, M. Weiler, O. Wertz, T. Wevers, Ł. Wyrzykowski, A. Yoldas, M. Žerjal, H. Ziaeepour, J. Zorec, S. Zschocke, S. Zucker, C. Zurbach, and T. Zwitter. Gaia Data Release 2. Summary of the contents and survey properties. A&A, 616:A1, Aug 2018. doi: 10.1051/0004-6361/201833051.

[15] A. Ginsburg, B. M. Sipőcz, C. E. Brasseur, P. S. Cowperthwaite, M. W. Craig, C. Deil, J. Guillochon, G. Guzman, S. Liedtke, P. Lian Lim, K. E. Lockhart, M. Mommert, B. M. Morris, H. Norman, M. Parikh, M. V. Persson, T. P. Robitaille, J.-C. Segovia, L. P. Singer, E. J. Tollerud, M. de Val-Borro, I. Valtchanov, J. Woillez, The Astroquery collaboration, and a subset of the astropy collaboration. astroquery: An Astronomical Web-querying Package in Python. AJ, 157:98, March 2019. doi: 10.3847/1538-3881/aafc33.

[16] Thomas Hockey, Virginia Trimble, Thomas R. Williams, Katherine Bracher, Richard A. Jarrell, Jordan D. Marché, F. Jamil Ragep, Joann Palmeri, and Marvin Bolt. *The Biographical Encyclopedia of Astronomers*. 2007. doi: 10.1007/978-0-387-30400-7.

[17] Dorrit Hoffleit. E. C. Pickering in the History of Variable Star Astronomy. *Journal of the American Association of Variable Star Observers (JAAVSO)*, 1:3, Jun 1972.

[18] Martin Horvat, Kyle E. Conroy, Herbert Pablo, Kelly M. Hambleton, Angela Kochoska, Joseph Giammarco, and Andrej Prša. Physics of Eclipsing Binaries. III. Spin-Orbit Misalignment. ApJS, 237(2):26, Aug 2018. doi: 10.3847/1538-4365/aacd0f.

[19] INDI Library. Indi library, 2019. URL `https://www.indilib.org/`.

[20] Lauri Jetsu and Sebastien Porceddu. Shifting Milestones of Natural Sciences: The Ancient Egyptian Discovery of Algol's Period Confirmed. *PLoS ONE*, 10:44140, Dec 2015. doi: 10.1371/journal.pone.0144140.

[21] Dustin Lang, David W. Hogg, Keir Mierle, Michael Blanton, and Sam Roweis. Astrometry.net: Blind Astrometric Calibration of Arbitrary Astronomical Images. AJ, 139(5): 1782–1800, May 2010. doi: 10.1088/0004-6256/139/5/1782.

[22] Latifah Maasarani. Astronomical Dome Automation using POTH ASCOM Platform. Technical report, University of Central Florida and University of Texas Rio Grande Valley, 2017.

[23] Curtis McCully, Steve Crawford, Gabor Kovacs, Erik Tollerud, Edward Betts, Larry Bradley, Matt Craig, James Turner, Ole Streicher, Brigitta Sipocz, Thomas Robitaille, and Christoph Deil. astropy/astroscrappy: v1.0.5 zenodo release, November 2018. URL `https://doi.org/10.5281/zenodo.1482019`.

[24] John R. Percy. *Understanding Variable Stars*. 2007.

[25] E. C. Pickering. Variable stars of short period. *The Observatory*, 4:225–231, Aug 1881.

[26] Edward Pigott. Observations of a New Variable Star. In a Letter from Edward Pigott, Esq. to Sir H. C. Englefield, Bart. F. R. S. and A. S. *Philosophical Transactions of the Royal Society of London Series I*, 75:127–136, Jan 1785.

[27] PlaneWave Instruments. 17 inch cdk optical tube assembly specifications page,

2019. URL http://planewave.com/products-page/telescopes/17-inch-cdk-optical-tube-assembly/.

[28] PlaneWave Instruments. Planewave software and updates, 2019. URL http://pw-ecommerce.com/software/.

[29] Sebastian Porceddu, Lauri Jetsu, Tapio Markkanen, and Jaana Toivari-Viitala. Evidence of periodicity in ancient egyptian calendars of lucky and unlucky days. *Cambridge Archaeological Journal*, 18(3):327–339, 2008. doi: 10.1017/S0959774308000395.

[30] Sebastian Porceddu, Lauri Jetsu, Tapio Markkanen, Joonas Lyytinen, Perttu Kajatkari, Jyri Lehtinen, and Jaana Toivari-Viitala. Algol as Horus in the Cairo Calendar: The Possible Means and the Motives of the Observations. *Open Astronomy*, 27(1):232–263, Sep 2018. doi: 10.1515/astro-2018-0033.

[31] A. M. Price-Whelan, B. M. Sipőcz, H. M. Günther, P. L. Lim, S. M. Crawford, S. Conseil, D. L. Shupe, M. W. Craig, N. Dencheva, A. Ginsburg, J. T. VanderPlas, L. D. Bradley, D. Pérez-Suárez, M. de Val-Borro, (Primary Paper Contributors, T. L. Aldcroft, K. L. Cruz, T. P. Robitaille, E. J. Tollerud, (Astropy Coordination Committee, C. Ardelean, T. Babej, Y. P. Bach, M. Bachetti, A. V. Bakanov, S. P. Bamford, G. Barentsen, P. Barmby, A. Baumbach, K. L. Berry, F. Biscani, M. Boquien, K. A. Bostroem, L. G. Bouma, G. B. Brammer, E. M. Bray, H. Breytenbach, H. Buddelmeijer, D. J. Burke, G. Calderone, J. L. Cano Rodríguez, M. Cara, J. V. M. Cardoso, S. Cheedella, Y. Copin, L. Corrales, D. Crichton, D. D'Avella, C. Deil, É. Depagne, J. P. Dietrich, A. Donath, M. Droettboom, N. Earl, T. Erben, S. Fabbro, L. A. Ferreira, T. Finethy, R. T. Fox, L. H. Garrison, S. L. J. Gibbons, D. A. Goldstein, R. Gommers, J. P. Greco, P. Greenfield, A. M. Groener, F. Grollier, A. Hagen, P. Hirst, D. Homeier, A. J. Horton, G. Hosseinzadeh, L. Hu, J. S. Hunkeler, Ž. Ivezić, A. Jain, T. Jenness, G. Kanarek, S. Kendrew, N. S. Kern, W. E. Kerzendorf, A. Khvalko, J. King, D. Kirkby, A. M. Kulkarni, A. Kumar, A. Lee, D. Lenz, S. P. Littlefair, Z. Ma, D. M.

Macleod, M. Mastropietro, C. McCully, S. Montagnac, B. M. Morris, M. Mueller, S. J. Mumford, D. Muna, N. A. Murphy, S. Nelson, G. H. Nguyen, J. P. Ninan, M. Nöthe, S. Ogaz, S. Oh, J. K. Parejko, N. Parley, S. Pascual, R. Patil, A. A. Patil, A. L. Plunkett, J. X. Prochaska, T. Rastogi, V. Reddy Janga, J. Sabater, P. Sakurikar, M. Seifert, L. E. Sherbert, H. Sherwood-Taylor, A. Y. Shih, J. Sick, M. T. Silbiger, S. Singanamalla, L. P. Singer, P. H. Sladen, K. A. Sooley, S. Sornarajah, O. Streicher, P. Teuben, S. W. Thomas, G. R. Tremblay, J. E. H. Turner, V. Terrón, M. H. van Kerkwijk, A. de la Vega, L. L. Watkins, B. A. Weaver, J. B. Whitmore, J. Woillez, V. Zabalza, and (Astropy Contributors. The Astropy Project: Building an Open-science Project and Status of the v2.0 Core Package. AJ, 156:123, September 2018. doi: 10.3847/1538-3881/aabc4f.

[32] A. Prša and T. Zwitter. A Computational Guide to Physics of Eclipsing Binaries. I. Demonstrations and Perspectives. ApJ, 628(1):426–438, Jul 2005. doi: 10.1086/430591.

[33] A. Prša, K. E. Conroy, M. Horvat, H. Pablo, A. Kochoska, S. Bloemen, J. Giammarco, K. M. Hambleton, and P. Degroote. Physics Of Eclipsing Binaries. II. Toward the Increased Model Fidelity. ApJS, 227(2):29, Dec 2016. doi: 10.3847/1538-4365/227/2/29.

[34] N. N. Samus', E. V. Kazarovets, O. V. Durlevich, N. N. Kireeva, and E. N. Pastukhova. General catalogue of variable stars: Version GCVS 5.1. *Astronomy Reports*, 61(1):80–88, Jan 2017. doi: 10.1134/S1063772917010085.

[35] Diffraction Limited / SBIG. *STF-8300 Specification Sheet*. Diffraction Limited / SBIG, 59 Grenfell Crescent, Unit B, Ottawa, ON K2G 0G3, Canada, 2019.

[36] C. Sterken and C. Jaschek. *Light Curves of Variable Stars, A Pictorial Atlas*. 1996.

[37] Peter B. Stetson. DAOPHOT: A Computer Program for Crowded-Field Stellar Photometry. PASP, 99:191, Mar 1987. doi: 10.1086/131977.

[38] The ASCOM Initiative. ASCOM Platform, 2019. URL `https://ascom-standards.org/index.htm`.

[39] Pieter G. van Dokkum. Cosmic-Ray Rejection by Laplacian Edge Detection. PASP, 113 (789):1420–1427, Nov 2001. doi: 10.1086/323894.

[40] Variable Star and Exoplanet Section of Czech Astronomical Society. Projekt B.R.N.O., August 2019. URL `http://var2.astro.cz/EN/brno/index.php?lang=en`.

[41] C. L. Watson, A. A. Henden, and A. Price. The International Variable Star Index (VSX). *Society for Astronomical Sciences Annual Symposium*, 25:47, May 2006.

[42] Stephen R. Wilk. Mythological Evidence for Ancient Observations of Variable Stars. *Journal of the American Association of Variable Star Observers (JAAVSO)*, 24(2):129–133, Jan 1996.

[43] Robert E. Wilson and Edward J. Devinney. Realization of Accurate Close-Binary Light Curves: Application to MR Cygni. ApJ, 166:605, Jun 1971. doi: 10.1086/150986.

[44] N. Zacharias, C. Finch, and J. Frouard. VizieR Online Data Catalog: UCAC5 Catalogue (Zacharias+ 2017). *VizieR Online Data Catalog*, art. I/340, Mar 2017.

BIOGRAPHICAL SKETCH

Moises Castillo, born in Brownsville, Texas and raised in Los Fresnos, Texas. Graduated from the pioneering class of the Math and Science Academy in 2009. Received a Bachelor of Science in Physics in 2012 from UTRGV legacy institution University of Texas at Brownsville. Received a Master of Science in Physics in August 2019 from UTRGV. Collaborator of the Dr. Cristina Valeria Torres Memorial Astronomical Observatory, Transient Optical Robotic Observatory of the South. Member of the American Association of Variable Star Observers and the American Physical Society.

Been part of the UTRGV Department of Physics since 2008. Worked as lab manager for the physics department from 2009-2014. Developed physics instructional laboratory manuals, instructional laboratory apparatuses, and instructional laboratory design and storage. Developed a physics outreach program with the Society of Physics Students in Brownsville. Presented physics concepts through large scale demonstrations to over ten thousand students of the Rio Grande Valley from McAllen to Santa Rosa to Brownsville and many schools in between. As an Outdoor Educator, instructed activities such as Canoeing and Archery and included physics concepts into all activities taught. Open to observation and critical feedback. Academic goal is to get a Ph.D. in Physics to supplement the professional goal for a place in academia. Email: castillo.moises11@gmail.com